



Review

Polymer-Based Materials Built with Additive Manufacturing Methods for Orthopedic Applications: A Review

Kunal Manoj Gide ¹, Sabrina Islam ¹ and Z. Shaghayegh Bagheri ^{1,2,*}

¹ Department of Mechanical Engineering, George Mason University, 4400 University Dr, Fairfax, VA 22030, USA

² KITE-Toronto Rehabilitation Institute, University Health Network, 550 University Ave, Toronto, ON M5G 2A2, Canada

* Correspondence: sbagheri@gmu.edu; Tel.: +1-703-993-5920

Abstract: Over the last few decades, polymers and their composites have shown a lot of promises in providing more viable alternatives to surgical procedures that require scaffolds and implants. With the advancement in biomaterial technologies, it is possible to overcome the limitations of current methods, including auto-transplantation, xeno-transplantation, and the implantation of artificial mechanical organs used to treat musculoskeletal conditions. The risks associated with these methods include complications, secondary injuries, and limited sources of donors. Three-dimensional (3D) printing technology has the potential to resolve some of these limitations. It can be used for the fabrication of tailored tissue-engineering scaffolds, and implants, repairing tissue defects in situ with cells, or even printing tissues and organs directly. In addition to perfectly matching the patient's damaged tissue, printed biomaterials can have engineered microstructures and cellular arrangements to promote cell growth and differentiation. As a result, such biomaterials allow the desired tissue repair to be achieved, and could eventually alleviate the shortage of organ donors. As such, this paper provides an overview of different 3D-printed polymers and their composites for orthopedic applications reported in the literature since 2010. For the benefit of the readers, general information regarding the material, the type of manufacturing method, and the biomechanical tests are also reported.

Keywords: 3D printing; polymer composites; bio-composites; implants; scaffolds; tissue engineering



Citation: Gide, K.M.; Islam, S.; Bagheri, Z.S. Polymer-Based Materials Built with Additive Manufacturing Methods for Orthopedic Applications: A Review. *J. Compos. Sci.* **2022**, *6*, 262. <https://doi.org/10.3390/jcs6090262>

Academic Editor:
Francesco Tornabene

Received: 12 July 2022
Accepted: 30 August 2022
Published: 8 September 2022

Publisher's Note: MDPI stays neutral with regard to jurisdictional claims in published maps and institutional affiliations.



Copyright: © 2022 by the authors. Licensee MDPI, Basel, Switzerland. This article is an open access article distributed under the terms and conditions of the Creative Commons Attribution (CC BY) license (<https://creativecommons.org/licenses/by/4.0/>).

1. Introduction

Musculoskeletal disorders such as osteoporosis, fragility fractures, and traumatic fractures are major health concerns in the United States (U.S.) because of the aging population, obesity, and sports injuries [1,2]. Several bone disorders cause degradation of bone strength and density, leading to bone fractures, such as Paget's disease, osteogenesis imperfecta, and rickets [2,3]. In the U.S. alone, almost 6.3 million bone fractures occur annually, costing the healthcare system USD 20 billion yearly [4], projected to reach USD 912 billion by the year 2025 [5]. These musculoskeletal disorders are treated using three primary methods, including auto-transplantation, xeno-transplantation, and implantation of artificial mechanical organs [1,6,7]. However, there exist some complications with each of these procedures. In auto-transplantation, grafting of a tissue or organ from one area of the body to another may lead to secondary complications and injuries [1,7]. Xeno-transplantation, restricted by limited donors, poses a risk of immunological rejection and viral transmission [1,8]. Although successful, there are issues associated with artificial implants like traditional methods of implant fabrication and materials [1,6], which lead to difficulty in producing complex geometries and human body rejection. Therefore, newer materials and fabrication techniques are being studied to overcome the limitations of artificial implants as fracture fixation devices or bone scaffolds.

In the selection of proper biomaterials for orthopedic applications, materials, and manufacturing methods are critical, which must be chosen based on the shape, cost, and performance requirements [6,9]. These materials can be grouped into three categories: metals, ceramics, and polymers. Metals like stainless steel [3,10,11] and cobalt-chrome alloys [3,12,13] were the first successfully used materials, followed by the growing popularity of titanium alloys and titanium implants in the 1940s [14,15]. For these metals, a variety of traditional manufacturing techniques are employed, including forging [16–18] and casting [19,20]. Metallic materials have a range of advantages, including biocompatibility, corrosion resistance, mechanical strength, and wear resistance [6,21], which make them attractive for orthopedic applications. One major disadvantage of using metals is their high elastic modulus, causing stress shielding [6,22,23]. This phenomenon occurs at the interface of the bone and the metal during load transfer, resulting in the newly repaired bone becoming less dense because of the removal of typical stress from the bone by the implant [6,22,23]. Other disadvantages of metals as raw materials for orthopedic applications include complexity in usage due to their radiopacity in computed tomography (CT) scans and magnetic resonance (MR) scans, as well as their release of toxic metal ions [21]. Another category of material currently being used is ceramics. Most common ceramic materials, such as alumina [24,25], calcium phosphate [26,27], zirconia [28–30], and glass ceramics [31,32], have shown excellent wear rates and corrosion resistance, superior biocompatibility, and high strength [3]. Despite these features, they are not well suited for load-bearing applications because of their less-favorable mechanical properties, such as low fracture toughness, brittleness, and high elastic modulus [3,32]. Similar to metals, ceramics have a high elastic modulus and are often observed to cause stress shielding, leading to complications such as a loss of bone mass [7,22] and loosening or failure of the implants [3,26].

Due to the disadvantages associated with making implants and bone scaffolds using metals and ceramics, polymers are becoming a more popular choice. The desirable material properties for these applications are the ability to be biocompatible, ease of molding, and durability [33,34], several of which are exhibited by polymers. Nylon, polyether-etherketone (PEEK), poly-ε-caprolactone (PCL), polymethylmethacrylate (PMMA), acrylic resins, polyurethanes, polypropylene (PP), ultra-high-molecular-weight polyethylene (UHMWPE), polyglycolic acid (PGA), polyethylene glycol (PEG), and polylactic acid (PLA) are a few of the polymeric materials that are currently being used in orthopedic applications [35–39]. Polymer materials in particular tend to have numerous advantages over metals and ceramics. By adjusting their composition, these materials can have their physical characteristics tailored to suit a variety of applications [3,33]. For instance, PEEK and its other co-polymers are attractive for orthopedic applications because of their similar mechanical properties to those of the bone as well as their good chemical resistance and radiolucency [39–41]. PCL is another good candidate that has been proposed in the field of bone tissue engineering [38,42,43]. Similarly, PMMA is used for a variety of orthopedic applications, such as craniofacial reconstruction and orthopedic spacers [36]. UHMWPE still represents the gold standard for arthroplasties due to its high fracture toughness and superior wear resistance [44–46]. The high water content of hydrogel makes it possible to achieve biphasic lubrication, resulting in low wear and very low coefficients of friction, making it a good material for artificial cartilage [6,37,47].

Despite the numerous advantages of polymeric materials, their clinical applications are still very limited due to the lack of mechanical stability for load-bearing purposes. To address this drawback, polymers have been combined with other materials to achieve enhanced properties [3,48,49]. Such combinations are known as composite materials, which are composed of at least two phases (matrix and fillers) with different physical or chemical properties, ranging from nano- to macro-sized [3,49–52]. Depending on the application, different types and distributions of filler materials in the matrix can produce various mechanical and biological properties [3,49]. For instance, ceramic/polymer composite bone scaffolds are designed to take advantage of the benefits of bioactive ceramics and the flexi-

bility of polymer when it comes to biological, mechanical, and physical properties. Some examples include PLA/hydroxyapatite (HA) scaffolds with better cell proliferation compared to PLA scaffolds [49,53–55], polylactic-co-glycolic acid (PLGA)/HA with enhanced mechanical properties for load-bearing orthopedic applications [56–59], and PEEK/HA composites with improved osseointegration and bone-implant interfaces [60–62].

Another important factor that affects the overall success of bone scaffolds and orthopedic implants is their microstructure and shape [63,64]. The morphology of a bone scaffold is of utmost importance, as it enables safe and rapid proliferation and differentiation of cells in all dimensions [63,64]. This morphology is influenced by the fabrication methods selected. There has been a variety of methods used to develop polymeric scaffolds in recent years, such as phase separation [64,65], electrospinning [66,67], freeze-drying [68], salt-leaching [69,70], melt-molding [71], and gas-foaming [72,73], whereas in the case of implants, casting, cutting, milling, forging, laser machining, and other conventional methods were used [16–20,74,75]. Although these methods have benefits, they all have certain drawbacks. The salt-leaching process not only leaves residual salts in the scaffolds but also results in irregular pore sizes [65]. Cell-seeding is inefficient with the freeze-drying process since closed-cell structures are formed in the matrix [65]. The pore size, one of the scaffold's important structural parameters, is not controlled in the gas-foaming method [76]. With the electrospinning method, there is still a problem with controlling pore size [77]. Conventional manufacturing of orthopedic implants, on the other hand, entails a loss of raw materials, the inability to produce accurate and complex structures, a longer waiting period, and higher costs [74,75]. These drawbacks lead to the need for improvement in the traditional fabrication methods. Consequently, regarding technological advancements in terms of the diversification of materials and improvement of dimensional accuracy, 3D printing (i.e., additive manufacturing (AM)) processes have been deemed a viable method for producing implants and bone scaffolds for orthopedic applications [9,35]. The adoption of additive manufacturing has enabled the creation of 3D structures with complex shapes as well as porous structures with controlled internal architecture. These were previously impossible through conventional manufacturing [9,78]. To manufacture scaffolds and implants, various AM methods are applied, including nozzle-based fused deposition modeling (FDM), resin-based stereolithography (SLA), and powder-based selective laser sintering (SLS) [35,78]. At first, a 3D model is created using computer-aided design (CAD) software such as SolidWorks, CATIA, Creo, and Fusion 360 or with the help of scans available through imaging [35,78,79]. Then this model is sliced into two-dimensional (2D) images using slicing software compatible with the 3D-printing machine [35,78,79]. The 2D images act as a guide for the printers to form each layer for the 3D models [35,79]. SLS can be used for polymers, metals, and ceramics. This method is known for its high precision and accuracy, as it depends on the laser and raw material. The laser fuses the powder in the desired shape layer by layer to form a 3D structure [9,34,78]. Another common method is SLA, which is known for its precision and speed, where ultraviolet (UV) light cures the raw materials, which are usually liquid photopolymers [34,35,80]. In the case of extrusion-based 3D printing, also known as FDM or fused filament fabrication (FFF), a filament usually made of a thermoplastic polymer is fed through a heated nozzle. This follows the desired shape of the object depositing material, which solidifies on cooling, layer by layer, to form a 3D object [34,78,79]. Binder jetting (BJ) is a method of manufacturing objects that utilizes a liquid bonding agent and powder-based materials. Three-dimensional objects are created using a print-head, which selectively jets a liquid agent according to the desired cross-section and glues powder materials together [81–83]. Even though these manufacturing methods are promising, they have their challenges and limitations, such as low surface quality, poor accuracy, low speed, limitation of part size, anisotropic mechanical properties, the building of overhang surfaces, high costs, low manufacturing efficiency, and limited use of materials [84–88]. In the case of FDM printing, only thermoplastic polymers or polymers reinforced with short fibers and particulates can be utilized, thereby limiting the range of raw material that can be used [84,85,88]. On the other hand, for SLA printing, the materials

are limited, as the process is based on photopolymerization, wherein the material is usually a composite mixture of epoxy or acrylate [84,88]. One of the drawbacks of SLS printing is that it cannot be utilized for creating closed structures, as the untreated powder is trapped inside the geometry [84,88–90]. In case of BJ, there is an additional post-processing step known as densification, which is required to cure the part, which is initially fragile [85,88]. A comparison of the different AM methods can be observed in Table 1 below. Another complication of the current AM method is the manufacturing errors that are inherent in these manufacturing techniques. These errors result in a geometry discrepancy between the designed and AM-printed parts, a dominant factor in contributing to manufactured samples with properties far from expected values. The problem is more serious in the applications that require complex geometries with specific internal features, such as porous bone scaffolds. A geometric mismatch can result in pore occlusion and walls with narrower thickness than the designed values, drawbacks that can inherently compromise bone ingrowth and severely impact mechanical performance [89,90]. Computational studies involving finite element analysis (FEA) help to analyze the deviation in the as-designed and as-manufactured parts, further proving the limitations of AM methods that need to be addressed [89–91]. Micromechanical modeling along with FEA analysis has been proposed as an effective and fast way to alter the properties of the material to desired values by using the resulting parameters as input for AM methods [91]. All of these AM methods have been successfully utilized in the field of orthopedic applications.

Table 1. Comparison between different AM processes discussed in the paper.

Method	Raw Material	Working Principle	Material Variety	Surface Finish	Processing Temperature	Production Speed	Part Property	Cost	Applications
FDM	Filament based	Filament extrusion	Polymer	Good accuracy	Low	Low	Moderate	Low	Automobile, aerospace applications, medical, education, piezo actuators, micro batteries
SLA	Liquid resin	Photopolymerisation	Polymer/resins	High accuracy	Very low	Low	Moderate	High	Architecture, bioengineering, jewelry industry, dental, education
SLS	Powder based	Powder bed fusion	Polymer/Ceramics/metals	Limited accuracy	High	High	High	High	Design prototype, structural components in aircraft, satellites, micro pumps
BJ	Liquid binding/powder based	Chemical bonding	Polymer/Ceramics/metals	Good accuracy	Low	High	Moderate	High	Figurines, sand-casting cores, molds, automotive, aerospace, art and design, architecture

Several papers have included discussions of the use of polymers and AM techniques in biomedical fields, but no comprehensive reviews are available on 3D-printed polymers and their composites, in particular for orthopedic applications. As such, this paper aims to provide a thorough review of the literature addressing different polymers used for orthopedic applications manufactured using AM processes since 2010. Most of the literature reviewed concerns the material properties and the fabrication method. For this review paper, the literature is organized into the different types of polymers and their composites. A detailed explanation of their method of fabrication, application, and material properties is given. Furthermore, each approach will be discussed in terms of its advantages and disadvantages.

2. Methods

Google Scholar and Pubmed were searched as follows: (a) Search terms were “3D printed polymer/composites” plus “mechanical/biological properties” plus “orthopedic

applications"; (b) experimental, computational, and clinical studies were searched for; (c) direct manufacturing of scaffolds and implants using 3D printing, rather than indirect manufacturing using 3D printed molds; (d) only orthopedic applications, rather than drug delivery and orthodontics; (e) studies since 2010; and (f) studies in English. Article reference lists were double-checked for additional studies.

3. Results

Recent advancements in AM technology have enabled the fabrication of biomaterials based on polymeric materials with a customized internal structure for orthopedic applications. Four types of polymer-based materials can be adopted for such applications, which are (i) natural polymers, (ii) synthetic polymers, (iii) hydrogels, and (iv) composites. Natural polymer constitutes both plant- and animal-derived polysaccharides, proteins, and polyesters [92]. Natural polymers including collagen [93–95], alginate [96–99], agarose [100–102], chitosan [102–108], fibrin [109,110], and hyaluronic acid-based materials [111–114] have been utilized over the years for various orthopedic applications. This includes scaffolds to repair subchondral cartilage defects, joint implants, and orthopedic fixation implants [47]. Despite having a positive effect on cell interaction with surrounding tissues, the clinical application of natural polymers is still very limited. The reason is their lack of availability in large quantities and the difficulty of processing them into bone scaffolds [47,103]. In the case of hydrogels, they are polymeric structures held together as water-swollen gels in different ways such as (i) covalent cross-links, (ii) ionic bonds, (iii) hydrogen bonds, (iv) bio-recognition interactions, (v) hydrophobic interaction, (vi) polymer crystallites, and (vii) physical entanglements [113–115]. Although they are being implemented as injectable scaffolds to fill irregularly shaped defects, their stiffness is still a cause of concern [47,113]. Man-made polymers, also known as synthetic polymers, are gaining a lot of interest in biomedical applications for their tailorable physical and chemical properties, achieved by a monomer unit, polymerization reaction, and/or cross-linking [116,117]. Currently, the most widely used polymers in orthopedic applications are PLA, PEG, PCL, PGA, and PEEK, to name a few [47,117].

3.1. Polylactic Acid (PLA)

PLA is an aliphatic polyester [118,119] that is derived from renewable natural resources such as corn starch, tapioca roots, and sugarcane [120]. It is biodegradable and melts at a lower temperature range of about 160–180 °C [120]. It is known for its good biocompatibility and mechanical properties [118,120–122], because of which it is a commonly used material for biomedical applications and has been approved by the U.S. Food and Drug Administration (FDA) for implantation in the human body [47,119,123–125]. This review article consists of 18 papers on PLA and its composites. Concerning mechanical properties of 3D-printed PLA scaffolds, there are two [120,126] studies reported in this literature, whereas two other studies [127,128] focused more on the parameters affecting cell adhesion and proliferation in PLA scaffolds. Only one study [118] reported the advantages of 3D-printing techniques over traditional manufacturing methods for scaffolds by analyzing the cell adhesion. Even though PLA is suitable as a polymer base for low-load-bearing applications, in the case of high-load-bearing applications its mechanical properties need to be enhanced [129]. This can be achieved via the addition of appropriate fillers in the polymer base, which has led to several studies in the field of PLA-based composites for orthopedic applications. Six papers [122,129–133] examined the effects of various fillers on the mechanical properties of the PLA-based composite scaffolds, and 10 [53,122–125,132–136] focused on the bioactivity of the composite scaffolds. Table 2 gives the range of properties recorded for PLA in this review. Table 3 summarizes the relevant results from every selected study based on PLA and its composites. The following studies are summarized in a manner that explains the process applied, the test conducted, and the results for the ease of the readers.

Table 2. Physical and mechanical properties of PLA and its composite material.

Material Properties	Value Range	Ref
Density	1.022–2.9 g/cm ³	[53,131]
Melting temperature	150–220 °C	[120,126,132]
Glass transition temperature	50–65 °C	[120,122]
Tensile strength	46.5–52 ± 6.7 MPa	[122,132]
Elongation at break	2.8–56%	[122,126]
Modulus of elasticity	0.00029–8.1 GPa	[125,129]
Yield strength	88–92.23 MPa	[130]
Compressive strength	4–46.11 MPa	[124,126]

Table 3. Mechanobiological literature of PLA and its composite material; C: compressive strength, T: tensile strength, D: displacement, Y: yield strength, E: modulus of elasticity, WCA: water contact angle, B: bending strength, R: roughness.

Mechanical Studies						
Ref	Filler	Manufacturing Methods	Type	Tests	Results	
[120]	N/A	FDM	Experimental	Tensile test Bending test	Ultimate load (tension): 572 N Ultimate load (bending): 97 N	
[129]	HA	FDM	Experimental	Nanoindentation test	E: 8.111 ± 0.714 GPa	
[131]	HA	FDM	Experimental FEA analysis	Compression test	C: 7.55 MPa E: 0.410 GPa Cylindrical cell structure prevented stress and crack propagation more effectively than the others	
Biological Studies						
Ref	Filler	Manufacturing Methods	Type	Tests	Results	
[128]	N/A	FDM	Experimental	In vitro	WCA: 24° R: 27.60 nm Increased cell adhesion and proliferation observed	
[127]	PDA	FDM	Experimental	In vivo In vitro	WCA: 11.2° Bone formation observed Good cell viability	
[134]	AW	Binder jetting	Experimental	In vivo In vitro	Cytocompatibility and new bone formation observed	
[123]	HA/BG	FDM	Experimental	In vitro	Cell adhesion and proliferation observed	
[135]	HA	FDM	Experimental	In vivo	Vascularized bone tissues prefabricated	
[136]	HA/eBM/IM	FDM	Experimental	In vivo	Enhancing bone repair and new bone formation observed	
Mechanobiological Studies						
Ref	Filler	Manufacturing Methods	Type	Tests	Results	
[126]	N/A	FDM	Experimental	Compression test pH meter In vitro	C: 46.11 MPa pH: 5.27 Cell adhesion and proliferation observed	
[118]	PDA/ BMP-2	FDM and Freeze-drying	Experimental	Nanoindentation test In vivo	E: 3.62 GPa Increased rate of bone repair was observed	

Table 3. Cont.

Mechanobiological Studies					
Ref	Filler	Manufacturing Methods	Type	Tests	Results
[122]	EFHA/FHA	FDM	Experimental	Tensile test In vivo In vitro	T: 46.5 ± 2.4 MPa E: 3.70 GPa WCA: $66.4 \pm 4.3^\circ$ Improved cell adhesion and proliferation observed
[130]	cHA/rGO	FDM	Experimental FEA analysis	Compression test In vitro	Y: 88–92.23 MPa Nontoxic with good biocompatibility and biodegradability
[132]	AMP	FDM	Experimental	Tensile test In vitro	T: 52 ± 6.7 MPa E: 2.07 GPa Enhanced cell adhesion and proliferation observed
[133]	HA/CS	FDM	Experimental	Bending test In vitro	Rapid growth in cell culture and proliferation observed
[124]	HA/CS	FDM	Experimental	Compression test In vitro	C: 4 MPa E: 50 MPa WCA: $38.1 \pm 2.9^\circ$ Cytocompatibility and proliferation observed
[125]	Halloysite/Zn	FDM	Experimental	Compression test In vitro	E: 0.29 MPa Enhanced cell adhesion observed
[53]	HA	FDM	Experimental	Compression Test In vivo In vitro	C: 23.36 MPa E: 0.6809 GPa New bone formation observed Cell adhesion and proliferation observed

With respect to the mechanical analysis, Burge et al. [120] used Taguchi L9 orthogonal array to design the experiment to find the optimum printing parameters, such as printing speed, infill percentage, layer height, and shell thickness for FDM-printed PLA scaffold. Based on the results from the mechanical tests, the order of significance of factors affecting tensile test was infill percentage, shell thickness, printing speed, and layer height, whereas for three-point bending, it was shell thickness, infill percentage, printing speed, and layer height. Dubinenko et al. [129] proposed ball milling using zirconia balls for the preparation of poly l-lactide (PLLA)/HA composite material for biomedical applications. Nanoindentation tests proved an enhancement in the Young's modulus with an increasing concentration of filler material. Sahmani et al. [131] conducted an experimental and computational analysis of FDM-printed PLA/HA scaffold to study the effects of internal cell architecture and pore sizes on its mechanical properties. Mechanical tests revealed higher values for compressive strength for samples with hexagonal than cubic or cylindrical porosities because of the higher elastic moduli. FEA proved that the cylindrical cell structure prevented stress and crack propagation more effectively than the others.

With respect to the biological analysis, Wang et al. [128] applied a cold atmospheric plasma (CAP) technique to modify the nanotopography of an FDM-printed scaffold to enhance cell adhesion, growth, and proliferation. Wang et al. [127] etched and coated the PLA FDM-printed scaffold using polydopamine (PDA) to study the effect of change in topography caused by etching on cell adhesion, growth, and proliferation. In vitro and in vivo tests showed enhanced cell proliferation, growth, cell viability, and bone regeneration capabilities of the etched and PDA-coated scaffold compared to the unetched scaffold. Tcacencu et al. [134] reported a composite of apatite-wollastonite (AW) and PLA structures created from a combination of BJ and FDM printing. The structures were thermally bonded to make the composite structure. In vitro assessment of the structures compared with a PLA or an AW structure revealed cytocompatibility of PLA, AW, and AW/PLA composites, whereas the in vivo assessment suggested that the AW/PLA composite had the largest amount of new bone formation. Alksne et al. [123] tried to improve osteoinductivity and

attenuate the adverse effect of degradation by comparing different PLA/HA and bioglass (BG)/PLA FDM-printed scaffolds. Absorption tests determined that the PLA/BG composite had a better absorption rate than the PLA/HA and pure PLA samples, whereas cell adhesion was weakest for the PLA/BG composite compared to PLA/HA and pure PLA. Zhang et al. [135] demonstrated prefabrication of FDM-printed PLA/HA scaffold large vascularized bone tissues using in vivo bioreactors. Liu et al. [136] proposed the use of induced membrane (IM) along with enhanced bone marrow (eBM) in a 3D-printed PLA/HA composite scaffold to treat long bone defects in vivo. The in vivo analysis showed that the combination of PLA/HA along with IM and eBM was able to treat the defect by enhancing bone repair and reconstruction.

With respect to the mechanobiological, Singh et al. [126] used a Taguchi L9 orthogonal array design of the experiment to study the effect of different process parameters such as infill percentage, infill pattern, and layer thickness on the mechanical and biological properties of FDM-printed PLA scaffolds. The compression test results showed a significant effect owing to the parameter in the study. A high infill percentage corresponded to a low drop in the compressive strength while hurting apatite formation. A lower infill percentage showed maximum bone cell growth and infiltration. Yao et al. [118] studied the enhancement in bioactivity and biocompatibility of a bone morphogenetic protein 2 (BMP-2)-coated FDM-printed scaffold by using PDA compared to a traditionally manufactured scaffold using freeze-drying. A nanoindentation test performed for analysis of mechanical properties revealed lower elastic moduli for FDM-printed scaffold compared to freeze-dried, suggesting a stronger bond with the bone tissue. In vivo CT observations proved an increased rate of bone repair and showed new bone tissue formation on the host bone and implant interface, which was significantly larger for FDM-printed BMP-2 coated scaffold. Wu et al. [122] reported the fabrication of fish-scale (sea bass)-derived HA (FHAP) and chicken eggshell (EGS) fillers in PLA matrix to study their effect on mechanical, thermal, structural, and antibacterial properties of FDM-printed scaffolds. Mechanical tests revealed an increase in the tensile strength and Young's modulus for both FHAP and EGS composites along with enhancement in thermal stability. Evaluation of the cytocompatibility of the composites showed better cell viability with enhanced cell aggregation for the FHAP composite than the EGS composite. Omigbodun et al. [130] conducted an experimental and computational analysis of PLA and carbonated HA (CHAP) along with reduced graphene oxide (rGO) to enhance the mechanical properties of FDM-printed scaffold with primitive and gyroid lattice structure. Analytical studies showed that gyroid lattice performed better for out-of-plane compression and shear test while being outperformed by primitive lattice for in-plane compression and three-point bending tests. The experiment demonstrated an increase in the mechanical properties of the composite material compared to the pure PLA scaffold. In vitro tests proved the composite scaffold was non-toxic and biocompatible, leading to better cell adhesion and growth. Elhattab et al. [132] applied the melt-blending technique to homogeneously disperse amorphous magnesium phosphate (AMP) in PLA to fabricate FDM-printed composite scaffolds. Mechanical testing revealed a reduction in the tensile strength and Young's modulus of both PLA and PLA/AMP composites after soaking in a phosphate buffer solution (PBS). This reduction was attributed to the degradation of the polymer and ceramic filler. In vitro testing demonstrated enhanced cell adhesion for the PLA/AMP composite than the PLA composite. Ranjan et al. [133] characterized the biological and mechanical performance using a flexural test and in vitro analysis of a PLA/HA/chitosan (CS) for an FDM-printed scaffold for biomedical applications. The results of all the measured values in the mechanical test were within considerable upper and lower critical limits for a bone scaffold. The biological results showcased rapid growth in cell culture, proving the biocompatibility of the composite configuration. Nazeer et al. [124] developed an FDM-printed PLA scaffold and modified its surface with CS and HA dispersed in formic acid to study its effect on the bioactivity of the composite scaffold. In vitro tests confirmed cell viability of the composite, proving CS/HA/PLA to be a better substrate for cell adhesion, migration, and growth. Luo et al. [125] proposed

the fabrication of an FDM-printed scaffold of PLA/halloysite nanotube (HNT)-loaded zinc nanoparticles (PLA/HNT/Zn) surface treated with two layers of fetal bovine serum (FBS) on the side and one layer of sodium hydroxide (NaOH) in the middle. Mechanical and in vitro test results showed enhanced mechanobiological properties for the composite compared to the pure material. Chen et al. [53] assessed the formation capacity of FDM-printed PLA/HA scaffold using an in vivo animal model. In vitro and in vivo tests results displayed enhanced cytocompatibility, cell adhesion, and new bone-forming ability of the PLA/HA composite scaffold.

3.2. Polyethylene Glycol (PEG)

PEG, also known as polyethylene oxide (PEO) [47], is a synthetic, well-known biocompatible polymer with hydrophilicity and solubility over a range of solvents [117,137]. Due to its higher molecular weight, PEG alone exhibits a higher compressive modulus [47]. It is nontoxic and possesses non-antigenicity and immunogenicity properties [138], which help to control the attachment of cells and proteins to its surface [47]. There are no studies reported on the use of PEG alone as implant materials for orthopedic applications, but six papers [137,139–143] have reported studies based on PEG composite in the same field. Table 4 gives the range of properties recorded for PEG in this review article. Table 5 also summarizes the relevant results from every selected study based on PEG composites.

Table 4. Physical and mechanical properties of PEG and its composite material.

Material Properties	Value Range	Ref
Melting temperature	56.5 °C	[142]
Modulus of elasticity	0.150–241.8 MPa	[137,142]

Table 5. Mechanobiological literature of PEG and its composite material; C: compressive strength, T: tensile strength, D: displacement, Y: yield strength, E: modulus of elasticity, WCA: water contact angle, B: bending strength, R: roughness.

Biological Studies					
Ref	Filler	Manufacturing Methods	Type	Tests	Results
[143]	PCL/ roxithromycin (ROX)	FDM	Experimental	Water-contact- angle analysis In vitro	WCA: 100.6 ± 3.7° Favorable for the prevention and treatment of bone infection
Mechanobiological Studies					
Ref	Filler	Manufacturing Methods	Type	Tests	Results
[139]	tECM	SLA	Experimental	Compression test In vivo In vitro	E: 0.3 MPa New bone formation observed Cell proliferation observed
[137]	PCL/MgO	FDM	Experimental	Compression test In vivo In vitro	E: 241.8 ± 16.6 MPa Early bone formation observed Cell proliferation observed
[140]	GelMA/HA/ PLGA/TGF- β1	SLA	Experimental	Compression test In vitro study	- Enhanced cell proliferation observed
[141]	nHA/RGDS	SLA	Experimental	Tensile test In vitro	E: 2.633 ± 0.218 MPa Increased cell proliferation and differentiation
[142]	ECM/ phytomolecule Honokiol	SLA	Experimental	Compression test In vivo In vitro	E: 0.150 MPa New bone and cartilage regeneration observed Suppress the release of proinflammatory cytokines from macrophages

With respect to the biological analysis, Bai et al. [143] experimented with melt electrohydrodynamic-printed composite scaffold made of PCL/PEG/roxithromycin (ROX). PEG added hydrophilicity to the composite, whereas ROX gave it antibacterial property proven by water-contact-angle tests and antibacterial assays. In vitro studies on the composite scaffold established good cell viability and growth.

With respect to the mechanobiological assessment of PEG and its composites, Luo et al. [139] combined polyethylene glycol diacrylate (PEGDA) with tendon extracellular matrix (tECM) to form a scaffold with enhanced porosity and strength using SLA printing. PEGDA provided physical and mechanical strength to the scaffold, whereas tECM was responsible for improving the biocompatibility of the synthetic polymer. In vivo test results showed a significantly high quality and a substantial quantity of new mineralized bone formation. Shen et al. [137] demonstrated the effect of the microenvironment on the efficacy of bone tissue regeneration on FDM-printed scaffolds of PCL-PEG-PCL composite treated with magnesium oxide (MgO) nanoparticles. Mechanical characterization showed a significant increase in compressive moduli of the composite. In vitro studies proved biocomposite scaffolds with a low concentration of magnesium ions (Mg^{2+}) in the microenvironment had excellent cytocompatibility and enhanced osteogenic differentiation. Early bone formation was observed in the composite scaffold compared to the control group. However, a large amount of Mg^{2+} in the microenvironment jeopardized the bone tissue regeneration ability of the scaffold. Zhou et al. [140] investigated the effect of an SLA-printed biomimetic, biphasic structure made of gelatin-methacrylate (GelMA) and PEGDA along with nHA and transforming growth factor beta-1 (TGF β -1) encapsulated in PLGA nanoparticles on osteochondral regeneration. Compressive test results proved to be inconclusive, as there was no significant difference observed between the modulus of elasticity of the different groups. In vitro analysis demonstrated enhanced cell proliferation for the composite material. Zhou et al. [141] studied the synergistic effect of low-intensity pulsed ultrasound (LIPUS) on the growth and osteogenic differentiation of human cells in SLA-printed scaffolds. Mechanical experimentation was performed to find the ideal pore size and porosity to increase cell proliferation. In vitro analysis of LIPUS-treated composite scaffolds presented a higher cell proliferation and differentiation than the control group. Zhu et al. [142] studied the effect of PEGDA/ECM along with the natural compound Honkiol (Hon) on regenerating osteochondral defects using SLA-printed scaffold. In vitro and histological analysis of the scaffolds revealed that PEGDA/ECM/Hon scaffolds suppressed the release of proinflammatory cytokines with significant enhancement in osteochondral regeneration. In vivo analysis of animal models exhibited new bone-formation capabilities.

3.3. Polycaprolactone (PCL)

PCL is a low-cost synthetic aliphatic polymer [144] that has been approved by the US FDA for tissue regeneration applications [145–150]. It is known for its biocompatibility as well as slow degradation rate [146,148,149,151]. The degradation rate of PCL contributes to its reduced cytotoxicity and inflammation in vivo [144,146]. Because of its low melting temperature (60 °C), it is easily printable using FDM technology and has moderate mechanical properties after manufacturing [145,148,152]. It has been applied as a cranial repair material and in other applications [148]. However, the application of PCL in bone tissue regeneration is limited due to its lack of bioactivity [42]. PCL is hydrophobic, because of which it is not favorable for cell adhesion and proliferation. Owing to this, few studies have been conducted on 3D-printed PCL for orthopedic applications [38]. Nevertheless, studies on PCL composite with various fillers to overcome its shortcomings are in abundance [42,43,144–164]. Table 6 gives the range of properties recorded for PCL in this review. Table 7 also summarizes the relevant results from every selected study based on PCL and its composites.

With respect to the clinical application, Han et al. [38] proposed the use of an FDM-printed patient-specific PCL biodegradable scaffold for the reconstruction of complex

maxillary defects. The implants were made after scanning the patient's head using a CT device and designed in commercial medical image-editing software. Post-operative follow-ups and CT analysis revealed tissue growth in the porous scaffold.

With respect to the mechanical characterization, Knutsen et al. [164] reported the static and fatigue properties of an SLS-printed PCL/HA cervical cage design of two kinds (i) a ring-shaped cage and (ii) a porous rectangular shape. Mechanical characterization by static and dynamic loading of the cages revealed that structural properties were affected by cage geometry and design. The optimized rectangular cage design performed better in the torsional test, whereas the ring-shaped design was better in compression tests.

With respect to the biological characterization, Kim et al. [42] evaluated the effect of alendronate (Aln)/PCL composite in bone tissue regeneration using FDM-printed scaffolds. In vitro studies indicated osteogenic differentiation, whereas in vivo animal tests proved increased new bone formation and bone mineralization. Xiong et al. [147] investigated the effect of adding transition metal nanoparticles to the mechanical and biological properties of an FDM-printed PCL/tantalum (Ta) scaffold. In vitro analysis for the biocompatibility of the PCL/Ta composite exhibited that increasing Ta content corresponded with better cell adhesion and proliferation. DeBaun et al. [157] aimed to develop an acellular technique where a PCL/ β -tricalcium phosphate (β -TCP) FDM-printed scaffold could be inserted into a long bone defect without an autologous bone graft. In vitro analysis proved that the PCL/ β -TCP with PMMA spacer performed better than the other group. In vivo tests demonstrated higher new bone formation properties. Li et al. [158] evaluated the osteogenic effect of freeze-dried platelet-rich plasma (PRP) on an FDM-printed PCL scaffold. In vitro analysis indicated enhanced cell proliferation and osteogenic differentiation. In vivo animal tests revealed the ability of the composite scaffold for greater new bone formation. Zhou et al. [159] fabricated an FDM-printed composite scaffold from PCL/PDA with vancomycin-loaded PLGA microspheres to enhance its antibacterial property. In vivo analysis confirmed that PDA coating enhanced cell proliferation. Lee et al. [161] demonstrated the effect of β -TCP in an FDM-printed PCL scaffold using a multi-head deposition system (MHDS). In vivo analysis showed new bone formation. Wu et al. [163] studied an FDM-printed PCL/calcium (Ca)/ECM composite scaffold for bone regeneration applications. The in vitro results concluded that the composite has excellent biocompatibility, cell adhesion, and proliferation. In vivo analysis displayed new bone formation capabilities of the scaffold. Zhao et al. [149] enhanced the osteoinductive and bioactivity of an FDM-printed PCL scaffold by incorporating magnesium (Mg). In vitro tests proved that the addition of Mg to PCL improved cell adhesion and proliferation. In vivo analysis of the animal model demonstrated that Mg increased the bioactivity of PCL scaffolds through increased osteointegration and new bone formation. Park et al. [160] proved that modified surface characteristics of FDM-printed PCL/HA scaffolds promote cell proliferation using alkaline treatment. They compared the effects of alkaline treatment using NaOH and oxygen (O_2) plasma treatment on the surface of PCL/HA composite. In vitro studies demonstrated enhanced cell proliferation on the NaOH-treated scaffold.

With respect to the mechanobiological characterization, Liu et al. [144] tested in vitro and in vivo FDM-printed scaffolds fabricated from PCL/HA. Compression testing proved that HA enhanced the compressive modulus of the PCL scaffold. In vitro test analysis showed the biocompatibility of PCL/HA and good cell proliferation. In vivo animal studies demonstrated bone regeneration capabilities. Amdjadi et al. [152] investigated the effects of surface-modified PEEK powder with a silane-coupling agent on the mechanical and biological properties of an FDM-printed PCL scaffold. The surface-treated PEEK created a hydrophilic surface for better adhesion to PCL. Compression tests demonstrated that PEEK addition greatly enhanced the mechanical properties of the composite scaffold at high porosities. In vitro tests on a PEEK/PCL scaffold exhibited enhanced adhesion and growth. Buyuksungur et al. [145] investigated the effect of FDM-printed PCL/HA scaffolds and polypropylene fumarate (PPF) on bone tissue regeneration via in vivo tests on rabbit femur defects. In vitro and in vivo test results displayed the biocompatibility of

the composite scaffold. Pandiyaraj et al. [146] reported using a non-thermal atmospheric plasma reactor for coating a porous FDM-printed PCL scaffold with triisopropyl phosphate (TIPP). In vivo tests showed enhanced bioactivity for the PCL/HA composite with the surface coating compared to the uncoated PCL/HA composite, thus supporting bone tissue regeneration. Ma et al. [148] compared the effects on FDM-printed scaffolds of different composite configurations such as PCL/polyvinyl acetate (PVAc), PCL, PCL/HA, and PCL/HA/PVAc through mechanical and biological characterizations. Mechanical characterization revealed that PCL/PVAc had the lowest compressive strength and modulus, whereas the PCL scaffold had the highest compressive strength and the PCL/HA scaffold had the highest modulus. In vitro assay proved that PCL/HA/PVAc showed the highest cell viability and proliferation along with the PCL/HA scaffold. In vivo analysis confirmed that PCL/HA/PVAc had higher new bone formation. Zhang et al. [43] compared the mechanical and biological properties of FDM-printed PCL scaffolds with and without bone marrow-derived human cells. Assessment of biomechanical properties showed high compressive and tensile strength in the composite PCL scaffolds. In vitro analysis of the composite scaffold revealed enhanced cell proliferation. In vivo analysis of animal models demonstrated new tissue formation. Golafshan et al. [153] fabricated magnesium phosphate doped with strontium ions (MgPSr) in an FDM-printed PCL implant to test its mechanical and biological properties. Mechanical characterization suggested enhanced properties of the composite material. In vitro analysis showed that Sr ions enhanced apatite formation, thereby increasing both the osteoinductive and osteoconductive properties. Radhakrishnan et al. [150] fabricated PCL/silver (Ag) nanoparticle FDM-printed scaffolds with antimicrobial properties for bone tissue-engineering applications. Mechanical characterization of the scaffold demonstrated increased the Young's modulus, which indicated the presence of Ag in the PCL matrix. In vitro analysis revealed that the addition of Ag reduced the degradation rate of the PCL composite. In vivo tests also confirmed that Ag promoted cell proliferation and cell viability. Abdal-hay et al. [151] investigated the approach to increase the bioactivity of an FDM-printed PCL scaffold by adding magnesium hydroxide (MH) nanoparticles. Mechanical tests showed a high tensile modulus and yield stress for the PCL/MH composite compared to the PCL-only scaffold. In vitro analysis proved enhanced osteoblast activity and biocompatibility. Hedayati et al. [155] utilized continuous fiber-reinforced FDM printing to fabricate a PCL scaffold with enhanced mechanical and biological properties. Mechanical characterization of the composite scaffolds revealed outstanding enhancement in the tensile strength and elastic modulus, whereas the in vitro analysis proved that continuous fiber reinforcement increased the degradation rate. Shim et al. [156] compared FDM-printed PCL and PCL/ β -TCP with conventional membranes for guided bone regeneration. Dry and wet mechanical tests revealed that conventional membranes were stronger in dry environments, but the composite performed better under wet conditions. In vitro analysis affirmed cell proliferation and inhibition of fibroblast ingrowth. In vivo analysis showed that composite PCL/ β -TCP performed better than the conventional collagen membrane. Nyberg et al. [162] compared FDM-printed PCL scaffolds loaded with different additives, which included β -TCP, HA, Bio-Oss (BO), and decellularized bone matrix (DCB). Mechanical testing proved that PCL/HA performed better than the other additives. In vivo studies revealed that PCL/BO and PCL/DCB scaffolds were advantageous in bone-healing applications. Xu et al. [165] assessed the bone reparability of PCL/BMSC/self-assembling peptide (SAP) 3D-printed scaffolds. In vitro results showed cell osteogenic differentiation in the composite scaffold. In vivo analysis confirmed the cell migration and wound-healing property of the scaffold.

3.4. Polyglycolic Acid (PGA) and Poly (Lactic-co-glycolic Acid) (PLGA)

PGA is a biodegradable aliphatic polyester [166,167] that can be synthesized through several processes such as polycondensation, ring-opening, and solid-state condensation [167,168]. Owing to its simple structure and stereochemistry, PGA can present a varying degree of crystallinity, from being completely amorphous to 52% crystallinity [169,170], resulting in

high mechanical properties and poor solubility in organic solvents [168]. Depending on the molecular weight of PGA, its mechanical and degradation properties can be controlled, making them suitable for a variety of applications [168]. On the other hand, PLGA is a copolymer composed of PLA and PGA [168,171]. It is approved by the FDA to be utilized as a biodegradable polymer for biomedical applications [171–173]. It can be synthesized by polycondensation of PLA and PGA or by ring-opening of PLA and PGA. It has excellent biocompatibility and processibility. The degradation rate and mechanical properties of PLGA can be controlled by varying the ratios of PLA and PGA, because of which it can be applied to several biomedical applications [172,174]. It also exhibits cell attachment, proliferation, and anchorage [171,175]. As PLGA and its composites offer much more flexible control over the degradation and mechanical properties, there are many research studies available for PLGA [172,175–181] compared to PGA and its composites [182,183]. Tables 8 and 9 give the range of properties recorded for PGA and PLGA in this review. Tables 10 and 11 summarize the relevant results from every selected study based on PGA, PLGA, and its composites.

Table 6. Physical and mechanical properties of PCL and its composite material.

Material Properties	Value Range	Ref
Melting temperature	52.9–72.3 °C	[43,155]
Tensile strength	4.96–79.7 MPa	[155,156]
Elongation at break	50–1342%	[151]
Modulus of elasticity	0.03374–3.5 GPa	[145,155]
Yield strength	5.44–7.8 MPa	[146,151]
Compressive strength	3.9–11.9 MPa	[148]

Table 7. Mechanobiological literature of PCL and its composite material; C: compressive strength, T: tensile strength, D: displacement, Y: yield strength, E: modulus of elasticity, WCA: water contact angle, B: bending strength, R: roughness, Tr: torsion.

Mechanical Studies					
Ref	Filler	Manufacturing Methods	Type	Tests	Results
[164]	HA	SLS	Experimental	Compression test Compression–shear test Torsion test	Compressive load: 650 N Compressive–shear load: 395 N Tr: 0.25 Nm
Biological Studies					
Ref	Filler	Manufacturing Methods	Type	Tests	Results
[42]	Aln	FDM	Experimental	In vivo In vitro	Bone tissue regeneration observed Cell proliferation and differentiation observed
[147]	Ta	FDM	Experimental	In vitro	Cell proliferation and bone formation observed
[157]	β-TCP	FDM	Experimental	In vivo In vitro	Improved bone tissue regeneration observed Cell proliferation observed
[158]	Platelet-rich plasma (PRP)	FDM	Experimental	In vivo In vitro	New bone formation observed Cell attachment, migration, proliferation increased
[159]	PLGA/PDA	FDM	Experimental	In vivo In vitro	New bone formation observed Cell proliferation increased
[161]	β-TCP	FDM	Experimental	In vivo	New bone formation observed

Table 7. Cont.

Biological Studies					
Ref	Filler	Manufacturing Methods	Type	Tests	Results
[163]	Calcium silicate (CS)	FDM	Experimental	In vivo In vitro	New bone formation observed Cell proliferation, adhesion, differentiation increased
[149]	Mg	FDM	Experimental	Water-contact-angle analysis In vivo In vitro	WCA: 75° Bone tissue regeneration observed Cell proliferation and differentiation observed
[160]	HA	FDM	Experimental	Water-contact-angle analysis In vitro	WCA: 62.2° Cell proliferation and differentiation increased
Mechanobiological Studies					
Ref	Filler	Manufacturing Methods	Type	Tests	Results
[144]	HA	FDM	Experimental	Compression test In vivo In vitro	E: 330 MPa New bone formation observed Cell proliferation observed
[152]	PEEK	FDM	Experimental	Compression test Water-contact-angle analysis In vitro	E: 76 MPa WCA: 69.4° Enhanced adhesion and growth observed
[145]	HA/PPF	FDM	Experimental	Compression test Tension test In vivo In vitro	Compressive Stiffness: 394 N/mm E: 33.74 MPa Tensile Stiffness: 463 N/mm WCA: 65° New bone formation observed Cell Proliferation observed
[146]	TIPP	FDM	Experimental	- Water-contact-angle measurement In vitro	E: 96.64 MPa Y: 5.44 MPa WCA: 11.5° Apatite formation observed
[148]	PVAc/HA	FDM	Experimental	Compression test In vivo In vitro	C: 3.9–11.9 MPa E: 125.4 MPa Cell proliferation and osteogenic activity observed
[43]	MSCs	FDM	Experimental	Compression test Tensile test In vivo In vitro	E(C): 135 MPa T: 24 MPa E(T): 130 MPa Bone tissue regeneration observed Cell proliferation and differentiation observed
[153]	MgPSr	FDM	Experimental	Compression test In vivo In vitro	Compressive Toughness: 375.5 kJ/m ³ Bone tissue regeneration observed Cell proliferation and differentiation observed
[150]	AgNps	FDM	Experimental	Tensile test In vitro	E: 0.35 GPa Degradation observed
[151]	MH	FDM	Experimental	Tensile test In vitro	E: 92.3 MPa Y: 7.8 MPa Increased degradation and enhanced osteoblastic activity observed

Table 7. Cont.

Mechanobiological Studies					
Ref	Filler	Manufacturing Methods	Type	Tests	Results
[155]	PGA	FDM	Experimental	Tensile test In vitro	T: 79.7 MPa E: 3.5 GPa 20% higher degradation observed
[156]	β -TCP	FDM	Experimental	Tensile test In vivo In vitro	T: 4.96 MPa E: 213.1 MPa Guided bone regeneration observed Cell proliferation observed Inhibition of external tissue ingrowth observed
[162]	TCP, HA, Bio-Oss (BO) (DCB)	FDM	Experimental	Compression test In vivo	E: 338 MPa Increased cell seeding and growth observed
[165]	BMSC/SAP	-	Experimental	Compression test In vivo In vitro	E: 45 MPa New bone formation observed Cell proliferation and differentiation increased

With respect to the biological characterization, Kim et al. [180] investigated the biocompatibility and bioresorption properties of the FDM-printed PLA/PGA copolymer membrane. In vivo analysis proved that the copolymer membrane performed better than the homopolymer in terms of biocompatibility and bioresorption. Kim et al. [183] utilized near-infrared fluorescence imaging to study in vivo degradation and cell tracking of FDM printed amino radical (NH₂)-functionalized PCL-PLLA-PGA copolymer scaffolds. In vivo evaluation proved new bone formation. Yang et al. [178] developed an FDM-printed scaffold of PLGA/HA and chitosan (HACC) for the treatment of infected bone repair. HACC prevented bacterial adhesion on the scaffold surface. In vitro and in vivo analysis suggested that the addition of HA into the PLGA scaffold increased cell attachment and proliferation along with neovascularization and tissue integration. Ma et al. [181] developed an Mg-based PLGA/TCP composite scaffold using an advanced low-temperature FDM printer. In vitro analysis revealed the release of Mg, inhibiting biofilm growth and bacterial adhesion. In vivo analysis exhibited new peri-implant bone formation. Wiria et al. [179] utilized BJ for PLGA/PGA scaffold fabrication to analyze its degradation and mechanical properties. The in vitro study conducted in PBS solution revealed that cell processes such as cell attachment, tissue growth, and host response depended on the degradation rate of the scaffold.

With respect to the mechanobiological characterization, Ding et al. [182] discussed an approach for regenerating a goat femoral head using a biphasic PLA/PGA and PCL/HA scaffold fabricated using SLA- and FDM-printing methods. Mechanical analysis indicated that the addition of PLA and HA in the respective polymers increased the mechanical properties of the composite. In vivo analysis of the animal models proved a good continuous and a homogenous layer of cartilage formation. Both scaffolds exhibited good biocompatibility and regeneration properties. Aragon et al. [172] fabricated PCL/PLGA scaffolds loaded with rifampicin using electrohydrodynamic printing for efficient prevention of infection and bone-regeneration purposes. In vitro cytocompatibility studies supported cell growth and bone regeneration. Babilotte et al. [175] developed and characterized an FDM-printed PLGA/HA composite scaffold for bone-regeneration applications. The tensile tests showed no significant change in the mechanical properties of the scaffold. In vitro analysis demonstrated good biocompatibility, cytocompatibility, cell viability, and proliferation and degradation properties of the composite scaffold. Liu and Webster [176] demonstrated the use of PLGA and nano-titania to mimic the macro- and nano-structure of the bone to promote bone cell function and enhance the mechanical properties of the composite scaffold.

They utilized an aerosol-based extrusion-printing method for the fabrication of the composite scaffold. Their results indicated that cell adhesion was the greatest for surface roughness close to that of the natural bone. In vitro analysis demonstrated osteoblast interactions with 3D scaffolds, bone cell infiltration, and proliferation. Han et al. [177] compared the effect on mechanical properties and degradation rates of FDM-printed poly (DL-lactide-co-glycolide) (PLDGA)/BG/biosilica (BS) scaffolds. Physiochemical and mechanical studies proved that the BS/PLDGA composite increased the degradation time and maintained its compressive strength for a longer duration than PLDGA/BG, which was more desirable for bone tissue repair applications.

Table 8. Physical and mechanical properties of PGA and its composite material.

Material Properties	Value Range	Ref
Modulus of elasticity	40 MPa	[182]

Table 9. Physical and mechanical properties of PLGA and its composite material.

Material Properties	Value Range	Ref
Tensile strength	0.7–2.6 MPa	[172,175]
Elongation at break	120–180%	[172]
Modulus of elasticity	2–260 MPa	[176,177]
Compressive strength	30–33 MPa	[177]
Yield strength	12 MPa	[177]

Table 10. Mechanobiological literature of PGA and its composite material; C: compressive strength, T: tensile strength, D: displacement, Y: yield strength, E: modulus of elasticity, WCA: water contact angle, B: bending strength, R: roughness.

Biological Studies					
Ref	Filler	Manufacturing Methods	Type	Tests	Results
[180]	PLA	FDM	Experimental	In vivo	Connective tissue formation and bone regeneration observed
[183]	PLLA/PCL	FDM	Experimental	In vivo In vitro	New bone formation observed Cell proliferation observed
Mechanobiological Studies					
Ref	Filler	Manufacturing Methods	Type	Tests	Results
[182]	PLA/PCL/HA	SLA/FDM	Experimental	Compression test In vivo	E: 40 MPa Cell proliferation, adhesion, differentiation increased New bone formation observed

3.5. Polyetheretherketone (PEEK)

PEEK is a polyaromatic semicrystalline thermoplastic [41,184] polymer that belongs to the poly-aryl-ether-ketone (PAEK) family [40,185]. It has developed into one of the first choices for load-bearing orthopedic applications because of its material properties, such as excellent biocompatibility and mechanical stability [186], thermal and chemical resistance, radiolucency, and low Young’s modulus [41,187–190]. With its mechanical properties close to those of human bone, a lot of research has been conducted on PEEK biomaterials for orthopedic applications [40,41,191–208]. One of the major drawbacks of PEEK polymer is its lack of osteointegration ability, as a result of which a lot of focus has been given to PEEK composites [21,61,185–188,190,209–216]. Table 12 gives the range of properties recorded for

PEEK in this review. Table 13 summarizes the relevant results from every selected study based on PEEK and its composites.

Table 11. Mechanobiological literature of PLGA and its composite material; C: compressive strength, T: tensile strength, D: displacement, Y: yield strength, E: modulus of elasticity, WCA: water contact angle, B: bending strength, R: roughness.

Biological Studies					
Ref	Filler	Manufacturing Methods	Type	Tests	Results
[178]	HA/Chitosan	FDM	Experimental	In vitro	Cell proliferation and differentiation increased
[181]	TCP/Mg	FDM	Experimental	In vivo In vitro	New bone formation observed Cell proliferation, viability increased
[179]	PGA	Binder jetting	Experimental	In vitro	Cell attachment, tissue growth affected by degradation
Mechanobiological Studies					
Ref	Filler	Manufacturing Methods	Type	Tests	Results
[172]	PCL	FDM	Experimental	Tensile test In vitro	T: 2.6 MPa E: 9 ± 4 MPa Cell proliferation, viability observed
[175]	HA	FDM	Experimental	Tensile test In vitro In vivo	T: 0.7 MPa New bone formation observed Cell proliferation, viability, differentiation increased
[176]	Nano-Titania	FDM	Experimental	Roughness analysis Tensile test In vitro	R: 100 nm E: 2 MPa Osteoblast adhesion increased
[177]	Bioglass/ Biosilica	FDM	Experimental	Compression test In vitro	C: 30–33 Mpa Y: 12 Mpa E: 190–260 Mpa Increased degradation observed

With respect to the clinical application, Wang et al. [41] analyzed clinical case studies for 3D-printed PEEK implants for the reconstruction of chest-wall defects in patients with chest-wall tumors. Their research proved the utility of 3D-printed PEEK implants for chest-wall reconstruction. Honigmann et al. [193] reported on in-hospital FDM-printed PEEK scaphoid prosthesis. They utilized medical-grade PEEK to successfully 3D print the scaphoid prosthesis in house using an FDM printer. Honigmann et al. [194] successfully FDM printed patient-specific implants from medical-grade PEEK filaments. They fabricated five different implants that passed the certified sterilization tests, thereby confirming the feasibility of manufacturing PEEK implants using 3D printing. Chen et al. [187] fabricated speech-aid prostheses using a PEEK filament supplemented with nano titanium oxide (TiO₂) powder by FDM printing. Clinical application of the prostheses exhibited precise fit and excellent mechanical properties and surface texture. Dong et al. [191] reported a case study wherein they investigated the effectiveness of 3D-printed PEEK prostheses for the treatment of benign fibrous histiocytoma of the scapula. The 3D-printed implant was fitted surgically in place of the resected bone because of the tumor. Post-operative X-rays revealed a satisfactory position of the left scapula as well as the shoulder joint. Therefore, this case study presented a successful clinical application of 3D-printed PEEK. Kang et al. [200] carried out an FEA to prove the utility of their design method for rib prostheses based on the centroid trajectory derived from a natural rib diaphysis using FDM-printed PEEK.

The resulting analysis provided proof that the new method could give better guidance for the design of the prostheses. Implantation of the prostheses achieved good clinical performance. Kang et al. [207] performed a clinical and computational biomechanical study using FEA for the reconstruction of the mandibular defect by combining FDM-printed PEEK and a free vascularized fibula graft. The deformation of the implant was lower than the actual deformation, which guaranteed stability. Clinical applications obtained excellent outcomes.

With respect to the mechanical characterization, Wang et al. [40] employed a design-of-experiments approach to evaluate the effects of printing parameters on FDM-printed PEEK on its mechanical properties for biomedical applications. Their results showed that nozzle diameter was the most significant parameter, followed by printing speed and nozzle temperature, which affected the mechanical properties of FDM-printed PEEK. Basgul et al. [204] explored the effects of printing speed and surface-treatment processes such as annealing on FDM-printed PEEK for lumbar spinal cage applications. Mechanical testing revealed no significant changes in mechanical properties for either annealing temperatures or lower mechanical properties for slower printing speed. Basgul et al. [192] studied the effect of changing layer-cooling time by varying nozzle diameter, printing speed, and the number of samples per print on interlayer bonding, mechanical properties, and porosity of FDM PEEK lumbar spinal cages. The layer cooling did not affect the interlayer adhesion. Mechanical tests revealed that bigger diameter nozzle cages were mechanically stronger as well as less porous. Basgul et al. [196] researched the effects of printing speed on the mechanical properties of 3D-printed PEEK for lumbar spinal cage applications. Mechanical tests performed on the cage structure revealed that stiffness decreased as the printing speed increased, but was in the range of 74–91% of the machined PEEK cage. Zhang et al. [205] designed a costal cartilage prosthesis using a wavy elastic structure of FDM-printed PEEK and optimized its biomechanical properties computationally using FEA. The tests revealed that the modulus and tensile strength of the FDM-printed PEEK prosthesis were close to those of natural costal cartilage. Guo et al. [197] performed FEA and mechanical experimentation to theoretically prove the usage of FDM-printed PEEK as a reconstruction material for repairing the temporomandibular joint. The computational analysis proved that properties of stress and strain were within the range of maximum yield strength of the material. Compression tests revealed uniform distribution of stress between bone and implant. Oladapo et al. [209], using FEA and mechanical experimentation, developed a surface characterization method for PEEK/HA/GO FDM-printed scaffold to improve its fracture toughness to resist crack propagation. Mechanical test results demonstrated that the presence of HA/GO in the PEEK matrix enhanced the mechanical properties, in particular, the fracture toughness.

With respect to the biological characterization, Han et al. [199] demonstrated the effect of surface roughness on the osteoblast response of FDM-printed PEEK implants for cranio-maxillofacial defects. In vitro analysis was performed on untreated, polished, and grit-blasted surfaces. The tests revealed that untreated surfaces exhibited better cell adhesion and proliferation than the polished or grit-blasted surfaces. Therefore, the study concluded that high surface roughness would provide better potential for cranio-maxillofacial defects. Sikder et al. [185] proposed the addition of AMP to enhance the bioactivity of FDM-printed PEEK implants. The in vitro results indicated that the addition of AMP particles resulted in superior pre-osteoblast functions as well as enhanced cell attachment, proliferation, and growth. In vivo analysis results corroborated the increased osteointegration property of the composite scaffold. Deng et al. [188] exhibited the dual potential of (AgNPs) as fillers in FDM-printed PEEK composite scaffolds to enhance their antibacterial and bioactive properties. In vitro analysis showed higher bioactivity of the composite PEEK scaffold than bare PEEK. Zhu et al. [210] presented a multifunctional FDM-printed PEEK/graphene scaffold with drug-laden HA to treat osteosarcoma and osteomyelitis. In vitro and in vivo tests revealed that HA increased the bioactivity of the scaffold while enhancing antibacterial properties. Deng et al. [211] constructed a hierarchical apatite/PDA/Ag/PDA coating on a 3D-printed PEEK scaffold for antibacterial purposes. Apatite increased the bone

ingrowth and osteointegration of the scaffold, as revealed by the *in vitro* and *in vivo* analysis. Elhatab et al. [201] reported on the effect of controlled microporosity by changing the infill percentages of FDM-printed PEEK on pre-osteoblast response. The *in vitro* test results indicated that the scaffolds with uniform macropores of around 800 micrometers (μm) had a high degree of cell attachment, growth, and proliferation because of their high surface area.

With respect to the mechanobiological assessment, Feng et al. [198] compared the effect of cross-linked structures (macropores) and acid-etched micropores of SLA-printed PEEK implants on their mechanical and biological properties. The compression tests performed revealed a decrease in compressive strength with increasing pore diameter. The *in vitro* test results indicated that macropores improved the ability of the PEEK implants to form a physical attachment with soft tissue, whereas the acid-etched micropores were beneficial for cell adhesion, growth, and proliferation. Zheng et al. [190] evaluated the influence of pore size, printing direction, and filler content on the mechanical properties of FDM-printed PEEK scaffolds. Varying compressive strength in different directions and the Young's modulus were obtained by changing the pore sizes. This resulted in controllability over the mechanical properties of the scaffold. *In vitro* analysis displayed increased cell attachment and mineralization because of the addition of HA particles. Oladapo et al. [186] studied the impact of different microstructures on FDM-printed PEEK/GO/HA composite hip implants. Mechanical tests confirmed that the scaffold with a ratio of PEEK 87 HA 10 and GO 3 exhibited optimal stress. Addition of HA and GO enhanced the bioactivity of the PEEK scaffold, as implied by *in vitro* analysis. Jung et al. [213] developed an FDM printer and optimized the printing parameters to successfully print PEEK scaffolds. The PEEK scaffolds were coated with titanium (Ti) using Ti sputtering. The printer and optimized settings increased the mechanical properties of the scaffold, whereas the titanium coating enhanced cell attachment, proliferation, and osteointegration, as proven by *in vitro* and *in vivo* analysis. Su et al. [202] improved the surface bioactivity of FDM-printed PEEK scaffolds by sulfonation treatment of the PEEK filament. This method created a microporous architecture, which enhanced the surface bioactivity of the PEEK structure. *In vitro* and *in vivo* tests showed that the sulfonated PEEK had improved adhesion, proliferation, and growth of bone-specific cells compared to untreated PEEK. Carpenter et al. [203] performed a computational study comparing the biomechanical performance of porous FDM-printed PEEK and titanium concerning their load sharing with bone using CT images of the implants with bone ingrowth. The tests revealed that porous PEEK exhibited greater load-sharing ability than titanium due to its elastic modulus being closer to that of human bone. In a study performed by Spece et al. [206], FDM-printed porous PEEK with different microarchitectures was evaluated for its osteoconductive properties. Mechanical as well as *in vitro* tests were carried out on the structures. The results confirmed that porous triply periodic minimal surface (TPMS) PEEK showed better osteoconductive and mechanical properties compared to the rectilinear structures. Li et al. [208] fabricated surface porous PEEK by FDM and performed mechanical and *in vitro* tests. The mechanical, theoretical, and numerical test results for the effects of pore diameter and pore layer number complied with each other. The *in vitro* tests exhibited better performance of surface porous PEEK with regards to cell adhesion and proliferation. Feng et al. [195] investigated the biological as well as mechanical properties of fully porous FDM-printed PEEK scaffolds with varying pore sizes. *In vitro* analysis showed excellent cell adhesion, proliferation, and osteogenic differentiation for PEEK scaffolds with 450 μm pore sizes. *In vivo* analysis of animal models showed new bone formations, as confirmed by MRI and micro-CT observations. Oladapo et al. [214] investigated the bioactivity of FDM-printed PEEK with cHA surface coating. Mechanical properties were increased because of the higher degree of crystallinity and accumulation of residual polymer. *In vitro* analysis proved that coating cHA on the PEEK surface enhanced apatite formation. *In vivo* tests also confirmed increased osteointegration and bioactivity. Oladapo et al. [215] suggested that GO and HA along with different microstructures affect the mechanical properties and bioactivity of FDM-printed

PEEK. The mechanical test results confirmed that an increase in the concentration of GO enhanced the mechanical properties, whereas in vitro tests showed that HA increased the bioactivity of the composite. FEA analysis showed that a body-centered cubic (BCC) octahedron lattice microstructure provided greater mechanical strength than other lattice structures. Manzoor et al. [216] studied the bioactivity and mechanical properties of FDM-printed PEEK and pure HA, HA doped with strontium (SrHA), and HA doped with zinc (ZnHA). Material characterization methods indicated the presence of HA and doped HA in the PEEK matrix. Thermogravimetric analysis confirmed that the addition of HA and doped HA increases the thermal stability of PEEK. Tensile test results displayed no significant difference in the Young’s modulus of the PEEK/HA composite for different doping agents, but the ultimate tensile strength was lower compared to pure PEEK. In vitro analysis proved increased bioactivity of PEEK/HA composite. Vaezi et al. [61] introduced a method capable of distributing HA in the PEEK matrix via a computer-controlled program, aiming to enhance its biological and mechanical properties. They prepared the HA bioceramic paste and FDM printed an interconnected HA phase. Compression molding was utilized to incorporate PEEK into the 3D-printed scaffold. Microscopy imaging found this method to be able to control pore size and distribution of the bioceramic phase in the PEEK matrix. The mechanical and in vitro test results displayed enhanced mechanobiological properties. Alam et al. [212] focused on an FDM-printed carbon nanostructure-reinforced PEEK composite for orthopedic applications. Increased crystallinity was observed in the PEEK composite material compared to the pure PEEK samples. Han et al. [21] compared the mechanical properties of FDM-printed carbon fiber-reinforced (CFR) PEEK with pure PEEK. Mechanical testing showed that CFR-PEEK had higher strength in general than pure PEEK samples. In vitro test results exhibited that surface topography made no difference in cell attachment on the surface of the PEEK and PEEK composite.

Table 12. Physical and mechanical properties of PEEK and its composite material.

Material Properties	Value Range	Ref
Density	1.181–1.868 g/cm ³	[40,215]
Melting temperature	334–400 °C	[40,209]
Glass transition temperature	139–149 °C	[216]
Tensile strength	8.3–143.7 MPa	[200,205]
Modulus of elasticity	0.017–34.96 GPa	[205,215]
Bending strength	19–193.33 MPa	[40,208]
Compressive strength	29.34–137.1 MPa	[21,209]
Yield strength	17.1–88 MPa	[206,207]

Table 13. Mechanobiological literature of PEEK and its composite material; C: compressive strength, T: tensile strength, D: displacement, Y: yield strength, E: modulus of elasticity, WCA: water contact angle, B: bending strength, R: roughness, Tr: torsion.

Mechanical Studies					
Ref	Filler	Methods	Type	Tests	Results
[41]	N/A	FDM	Experimental	Tensile test Bending test	T: 89 MPa B: 141 MPa E: 2.8 GPa
[40]	N/A	FDM	Experimental	Compression test Bending test	C: 87 MPa E: 2.098 GPa B: 193.33 MPa
[204]	N/A	FDM	Experimental	Compression test Compression–shear test	Compressive stiffness: 8874 N/mm Compressive–shear Stiffness: 1335 N/mm
[192]	N/A	FDM	Experimental	Compression test	Ultimate load for C: 11,686 N

Table 13. Cont.

Mechanical Studies						
Ref	Filler	Methods	Type	Tests	Results	
[196]	N/A	FDM	Experimental	Compression test Compression–shear test Torsion test	Compressive stiffness: 9324 N/mm Compressive–shear stiffness: 929 N/mm Tr: 1.37 Nm/deg	
[205]	N/A	FDM	Experimental FEA analysis	Tensile test	T: 8.3 MPa E: 17.3 MPa	
[207]	N/A	FDM	Experimental FEA analysis	Tensile test Flexure test	E: 2.8 GPa Von Mises: 366.5 MPa Y: 88 MPa B: 76 MPa	
[197]	N/A	FDM	Experimental FEA analysis	Compression test	Von Mises (screws): 9.71 MPa Von Mises (condyle): 10.33 MPa	
[200]	N/A	FDM	Experimental FEA analysis	Tensile test Bending test	T: 143.7 MPa B: 76.0 ± 23.7 MPa	
[209]	HA/GO	FDM	Experimental FEA analysis	Compression test Tensile test	C: 29.34 MPa T: 102.38 MPa E: 2.43 GPa B: 132.37 MPa	
Biological Studies						
Ref	Filler	Methods	Type	Tests	Results	
[199]	N/A	FDM	Experimental	In vitro	R: 26.7 μm Cell attachment, growth, and proliferation observed	
[185]	AMP	FDM	Experimental	In vivo In vitro	Enhanced bioactivity and superior pre-osteoblast cell function observed Enhanced osseointegration observed	
[188]	AgNPs	FDM	Experimental	In vitro	Cell attachment, growth, and proliferation observed	
[210]	Graphene/HA	FDM	Experimental	In vivo In vitro	New bone growth observed Cell attachment, growth, and proliferation observed	
[211]	AgNPs/pDA	FDM	Experimental	In vivo In vitro	New bone growth observed Cell attachment, growth, and proliferation observed	
[201]	N/A	FDM	Experimental	Water-contact-angle analysis In vitro	WCA: 39° Cell attachment, growth, and proliferation observed	
Mechanobiological Studies						
Ref	Filler	Methods	Type	Tests	Results	
[190]	HA	FDM	Experimental	Compression test In vitro	E: 112 MPa (Z-axis) 124 MPa (X-axis) Increased cell attachment and mineralization observed	
[186]	GO/HA	FDM	Experimental FEA analysis	Tensile test In vitro	Von-Mises stress: 25.32 GPa Cell attachment, growth, and proliferation observed	

Table 13. Cont.

Mechanobiological Studies						
Ref	Filler	Methods	Type	Tests	Results	
[213]	Ti	FDM	Experimental	Tensile test In vivo In vitro	T: 84.1 MPa Y: 78.7 MPa E: 2.42 GPa New bone growth observed Cell attachment, growth, and proliferation observed	
[202]	N/A	FDM	Experimental	Compression test In vivo In vitro	C: 36.20 MPa E: 575 MPa Newly-regenerated soft tissues adhesion observed Cell attachment, growth, and proliferation observed	
[203]	N/A	FDM	FEA analysis	Compression test Tensile test Shear test Bone tissue-strain study	82.3% load shared Majority of the load is carried by the bone with peek Favorable bone ingrowth properties found	
[206]	N/A	FDM	Experimental	Compression test In vitro	Y: 17.1 MPa E: 210–268 MPa Cell attachment, growth, and proliferation observed	
[208]	N/A	FDM	Experimental	Tensile test Bending test In vitro	T: 29–39 MPa Y: 85.23 MPa B: 19–29 MPa Cell attachment, growth, and proliferation observed	
[195]	N/A	FDM	Experimental	Compression test In vivo In vitro	C: 102.7 MPa E: 1006.5 MPa New bone formation observed Cell attachment, growth, and proliferation observed	
[214]	cHA	FDM	Experimental	Tensile test In vitro	T: 97.08 MPa E: 3.4 GPa Cell attachment, growth, and proliferation observed	
[215]	rGO/cHA	FDM	Experimental FEA analysis	Compression test Tensile test In vivo In vitro	Von Mises stress: 25,000 MPa T: 100 MPa E: 34.96 GPa Osseointegration activity observed Cell attachment, growth, and proliferation observed	
[216]	HA/Sr/Zn	FDM	Experimental	Tensile test In vitro	T: 51.5 MPa E: 785.9 MPa Cell attachment, growth, and proliferation observed	
[61]	HA	FDM/ compression molding	Experimental	Compression test In vitro	C: 110 MPa E: 2.5 GPa Good biocompatibility and cell attachment	

Table 13. Cont.

Mechanobiological Studies						
Ref	Filler	Methods	Type	Tests	Results	
[212]	CNS/GNPs	FDM	Experimental	Tensile test In vitro	T: 86.54 MPa Y: 77.69 MPa E: 3.96 GPa Cell attachment, growth, and proliferation observed	
[21]	CFR	FDM	Experimental	Compression test Tensile test Bending test In vitro	C: 137.1 MPa T: 101.41 MPa E: 7.37 GPa B: 159.25 MPa Cell attachment, growth, and proliferation observed	
[198]	N/A	SLA/injection molding	Experimental	In vitro	Cell attachment, growth, and proliferation observed	

There is a continuous development of new materials for orthopedic applications. These developments can be brought about by finding materials or altering the formulation of existing materials. Apart from the materials discussed in detail above, there are still a few other materials that are currently being used for orthopedic applications, such as poly-para-dioxanone (PDS), polyhydroxybutyrate (PHB), polytetrafluoroethylene (PTFE), polyethylene terephthalate (PET), and polyethylene (PE).

4. Discussion

Several polymers built with AM process have been considered for orthopedic applications in the recent years. In this article, we provide a comprehensive review of the literature relating to these polymers since 2010. Numerous insightful findings can be discerned from the selection of studies regarding the use of 3D-printed polymers and their biocomposites for orthopedic applications. On the other hand, even with improvements achieved by the wide variation in the different approaches taken for the manufacturing and testing by each study, future research is required to overcome the many remaining limitations, such as narrow selection of materials and manufacturing methods, the bioactivity of the material, etc. From the information in this review, several key points can be utilized to further the research on 3D printing polymers and their biocomposites for orthopedic applications.

First, having the relevant data from research summarized in a review such as this provides clinicians and biomedical engineers with a reference for choosing the materials, manufacturing methods, and testing parameters. Tables 2–13 provide summarized literature on these biomaterials. For reference, it lists the most common polymer and various fillers for their biocomposites, manufacturing methods, and tests performed, along with results that can be utilized for future research.

The cost, intended application, or purpose of the part are some of the parameters to look for during the selection of the materials. The manufacturing method and material selection are dependent, as there is a limitation on which material can be manufactured using a particular manufacturing method. For instance, PEEK used to be only printable by SLS, but recent advances in FDM have enabled the fabrication of PEEK. Figure 1 displays the range of properties that are reported in the literature for a given material and manufacturing method. These data can be utilized to model a specific part with the required performance. It is evident from Figure 1 that PLA-based and PEEK-based materials display a wide range in their elastic modulus and can be manufactured using FDM, whereas in case of PEG and PGA/PLGA both FDM and SLA methods can be utilized to manufacture a part with a similar elastic modulus. The variation in the range of mechanical properties that is reported for PEEK-based and PLA-based materials is because of the addition of different types of fillers, such as HA and CF, which alter their performance. A similar trend is also observed

in Figure 1B–E, where the respective mechanical properties of FDM-printed PEEK are spread over a wide range of values owing to the type and composition of the polymer.

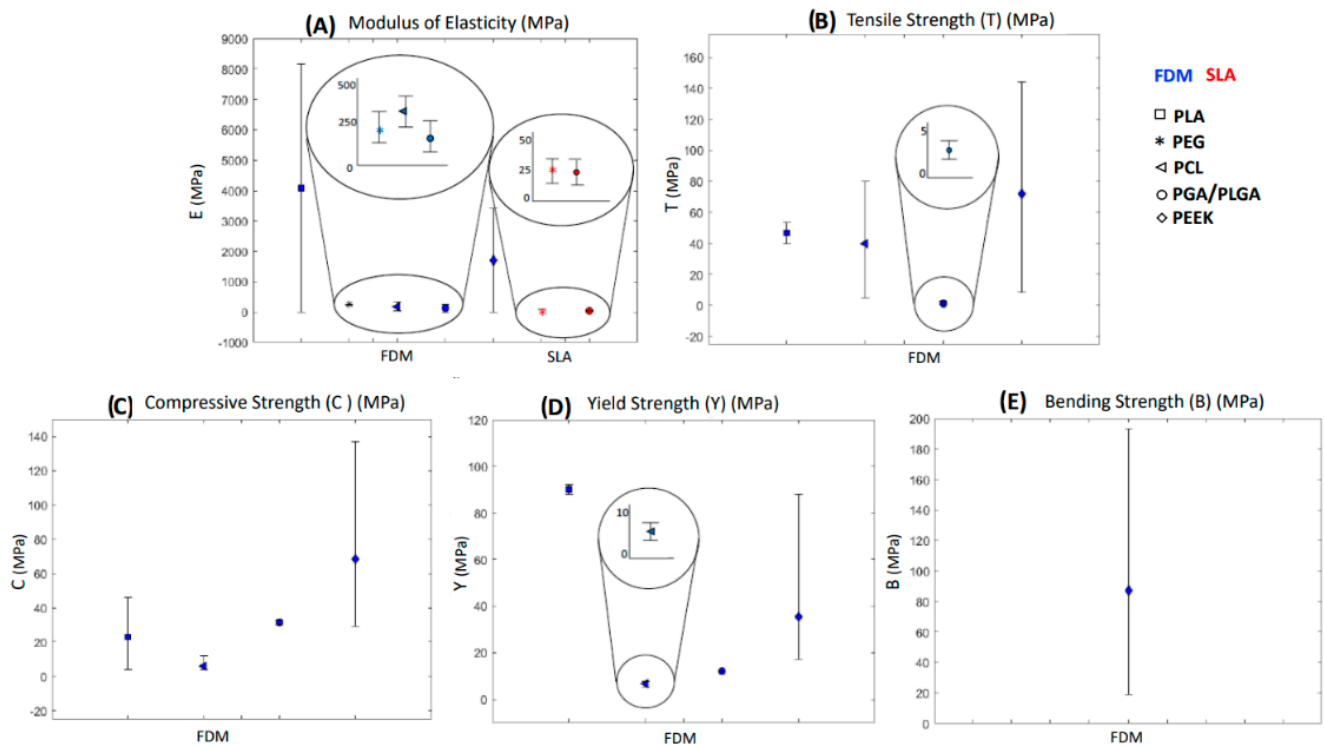


Figure 1. Mechanical properties reported vs. AM method reviewed. (A) Modulus of elasticity; (B) tensile strength; (C) compressive strength; (D) yield strength; (E) bending strength. Blue markers are for FDM, and Red Markers are for SLA. (For interpretation of the references to color in this figure legend, the reader is referred to the web version of this article).

Second, 3D printing was initially utilized in engineering and not for orthopedic clinical applications. Although in recent years there has been an increase in the development in this area, it still requires further research. As engineering and orthopedics are separate fields of study, there are no set standards that can be followed. As such, there are scattered results in the reviewed literature on the mechanobiological properties of the implants and scaffolds due to a huge variety in the testing methods and scope. These variations include different cells and animal models used for in vitro and in vivo analysis, respectively, for biological properties and different standards for mechanical properties. Additionally, international standards for the selection of 3D-printing materials for orthopedic purposes have not yet been developed. Typical research questions that need to be further studied in this effort might include the following: (1) Which materials are suited for both 3D printing as well as orthopedic applications? (2) What are the minimum mechanobiological properties required for successful application in the desired field? (3) What are the different models required for in vitro and in vivo analysis as well as standardizing the tests for mechanical testing? The answer to these research questions will help to standardize the material and manufacturing-process selection as well as mechanobiological testing protocol for orthopedic applications and will provide a more uniform platform to compare different studies.

Specifically, concerning the first question posed above, Tables 2–13 group the studies accordingly with the 3D-printing method suited to the material for the given applications. Although the studies in this review are focused on some of the most common synthetic polymers and their composites, further research is still needed to incorporate more biocompatible 3D-printable materials. Tables 2–13 also consist of the tests performed to measure the mechanobiological properties of the material along with the results. Overall, this can serve as a guide for future experiments in the desired area.

Third, some polymers have not been discussed here, such as poly-para-dioxanone (PDS), polyhydroxybutyrate (PHB), polytetrafluoroethylene (PTFE), polyethylene terephthalate (PET), and polyethylene (PE). This is due to inadequately published studies on the utilization of these polymers. Although these polymers are infrequently used, they still require baseline research to establish clinical recommendations for their application.

Concerning bone scaffolds, this paper reviews 72 studies focusing on the mechanical and/or biological properties of 3D-printed orthopedic scaffolds out of the total 93 papers that are reviewed in this paper. Among them, 10 used pure polymers to manufacture scaffolds. Compared to other manufacturing methods discussed in this review, most studies employed FDM printing to manufacture scaffolds due to its advantages, including reduced cost and a wide choice of materials. There is a similar distribution of the use of PLA, PCL, PEEK, and their composites in the literature. The physical properties of the scaffolds, such as porosity and pore size, were, in turn, in the range of 25–88% as well as 200–900 μm. These ranges are well within the range specified in the literature for cell adhesion and proliferation. Based on biological testing performed on the scaffolds, such morphological features (i.e., porosity and pore size) contributed to an enhancement in their biological properties. Despite the success of polymeric materials in orthopedic applications, there is still a need for continuous improvement in the development of materials in terms of biocompatibility, durability, and mechanical properties. Polymers are generally bioinert; as such, they need to be combined with bioactive filler for this purpose. According to the reviewed articles in the current study, HA is the most popular filler material due to its capacity to increase polymer bioactivity.

Concerning implants, 21 reviewed studies were devoted to 3D-printed implants for orthopedic applications, 14 of which employed pure polymers for their fabrication. The majority of implants were made from PEEK and its composites. The utilization of PEEK and its composites for manufacturing implants can be attributed to its higher mechanical properties compared to the rest of the reported materials. The most common method of manufacturing implants was through FDM printing. The remaining two studies focused on the properties of the material to be utilized in orthopedic applications. Figure 2A,B briefly summarizes the data reviewed in the paper based on the polymer and manufacturing methods.

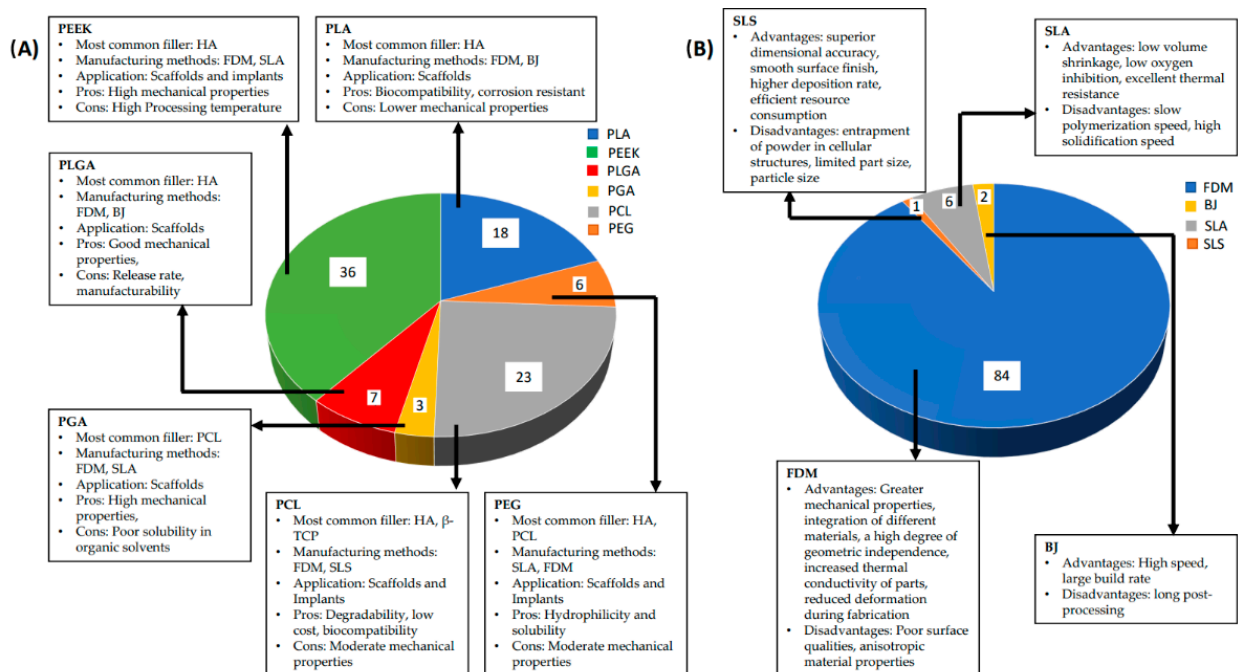


Figure 2. Pie chart. (A) Number of studies of each polymer available in the literature. (B) Number of times the AM method is used in the literature. (For interpretation of the references to color in this figure legend, the reader is referred to the web version of this article.)

Figure 3 represents the graph for the combined mechanical properties exhibited by the polymers and their composites reviewed in this article. As depicted in Figure 3a, we can see the wide range of elastic moduli recorded in the studies, from 0.150 MPa for PEGDA to 34.96 GPa for PEEK composite. This vast difference is attributed to the different types and ratios of filler material to manufacture the composites. A similar trend is observed in Figure 3b–d, where the respective mechanical properties are spread over a wide range of values owing to the type and composition of the polymer. This could be beneficial, as it provides a map for designing the implant or scaffold with the desired property range suitable for a particular application with appropriate material. Bending-strength values were only reported for studies done on PEEK and its composites, as represented in Figure 3e. This can be attributed to the rest of the polymers reviewed having considerably lower bending strength than PEEK. Two other studies performed flexural tests for PLA; however, no values were reported.

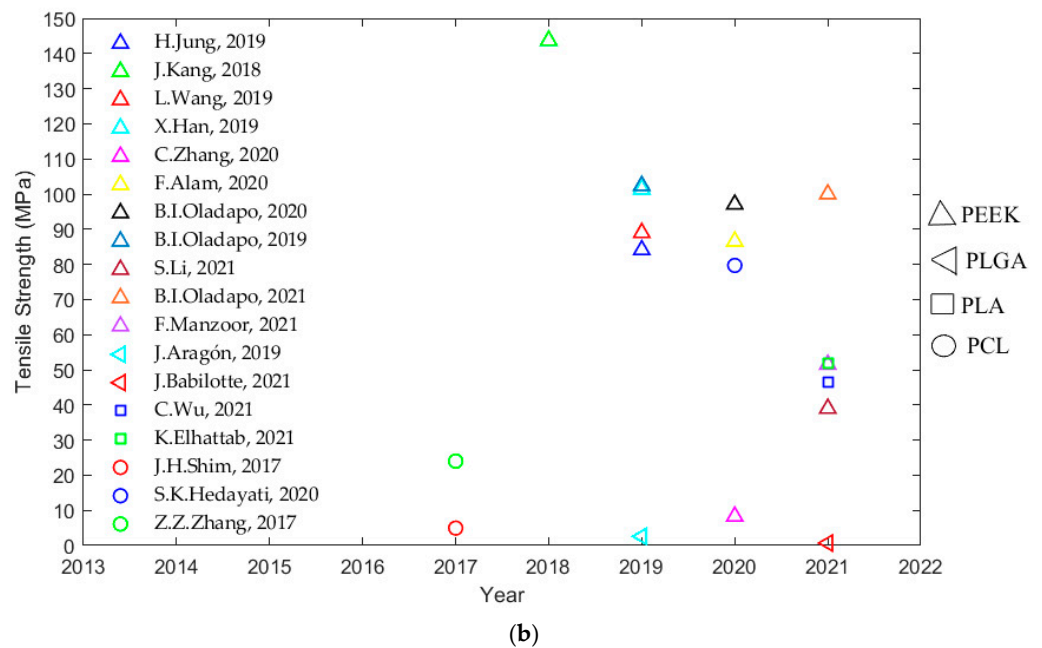
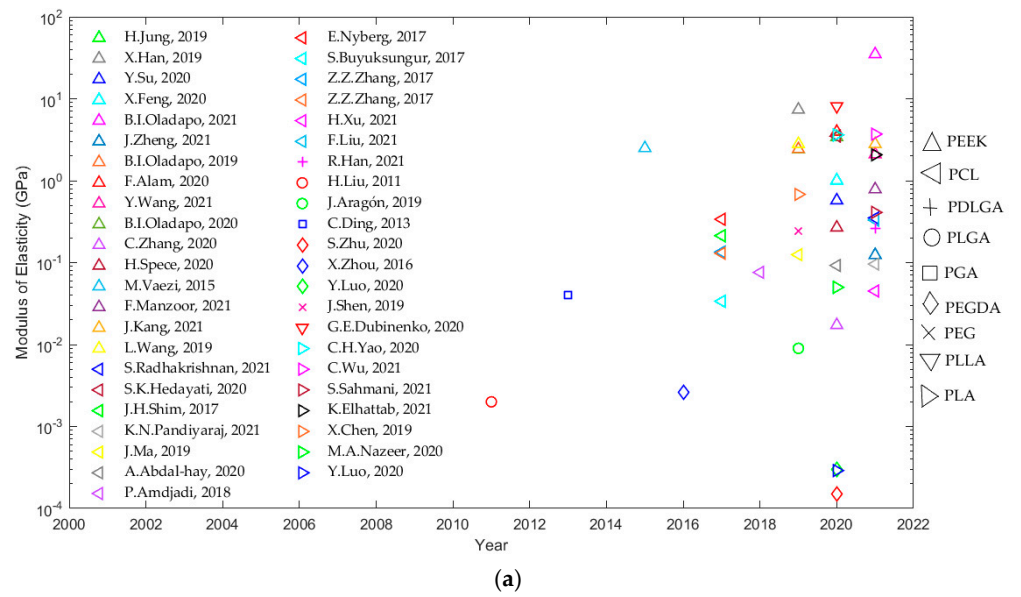
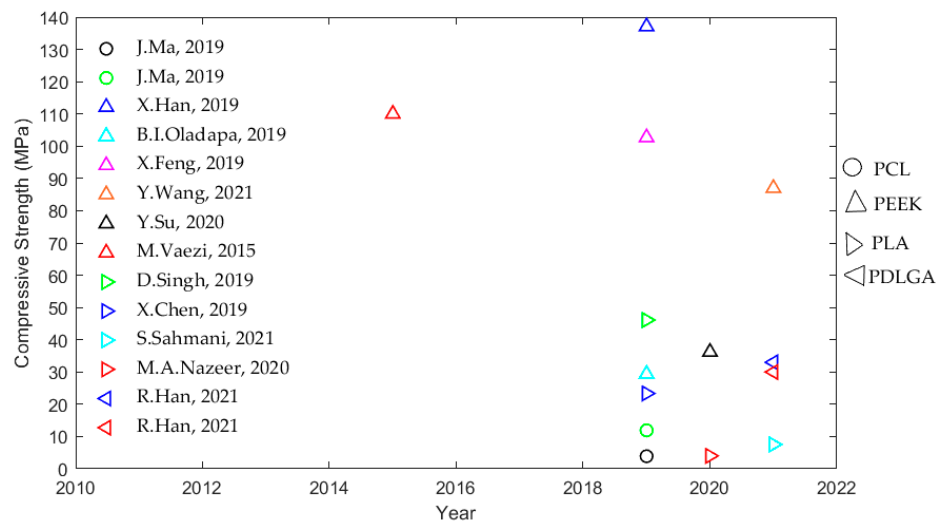
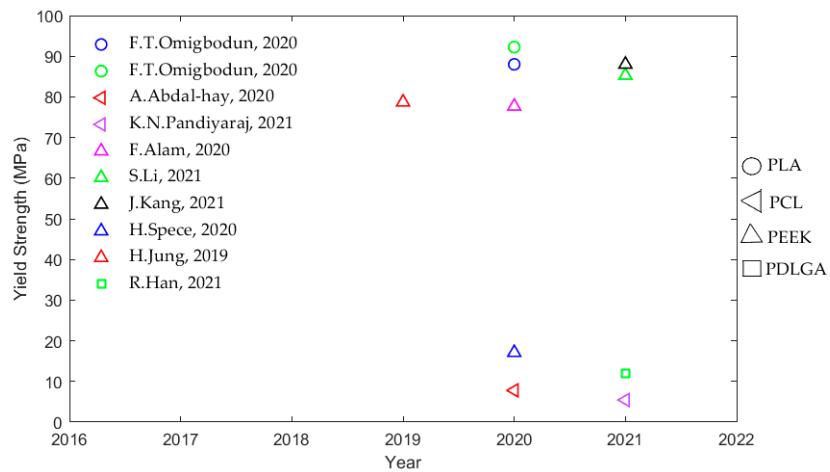


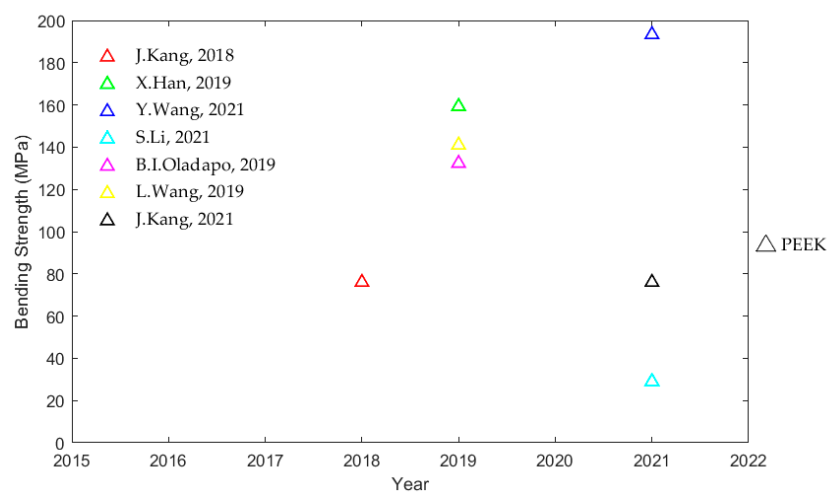
Figure 3. Cont.



(c)



(d)



(e)

Figure 3. The combined values of mechanical properties for each polymer and composites recorded in the studies reviewed in this article vs. the year of publication. (a) Modulus of elasticity (GPa); (b) tensile strength (MPa); (c) compressive strength (MPa); (d) yield strength (MPa); (e) bending strength (MPa). (For interpretation of the references to color in this figure legend, the readers are referred to the web version of this article).

Figure 4 represents the summarized diagram of the clinical applications in the studies reviewed in this paper. As can be seen by the limited numbers of these clinical studies being reported, there is still a lot to be done to utilize 3D printing and polymer/composites in the field of orthopedic applications.

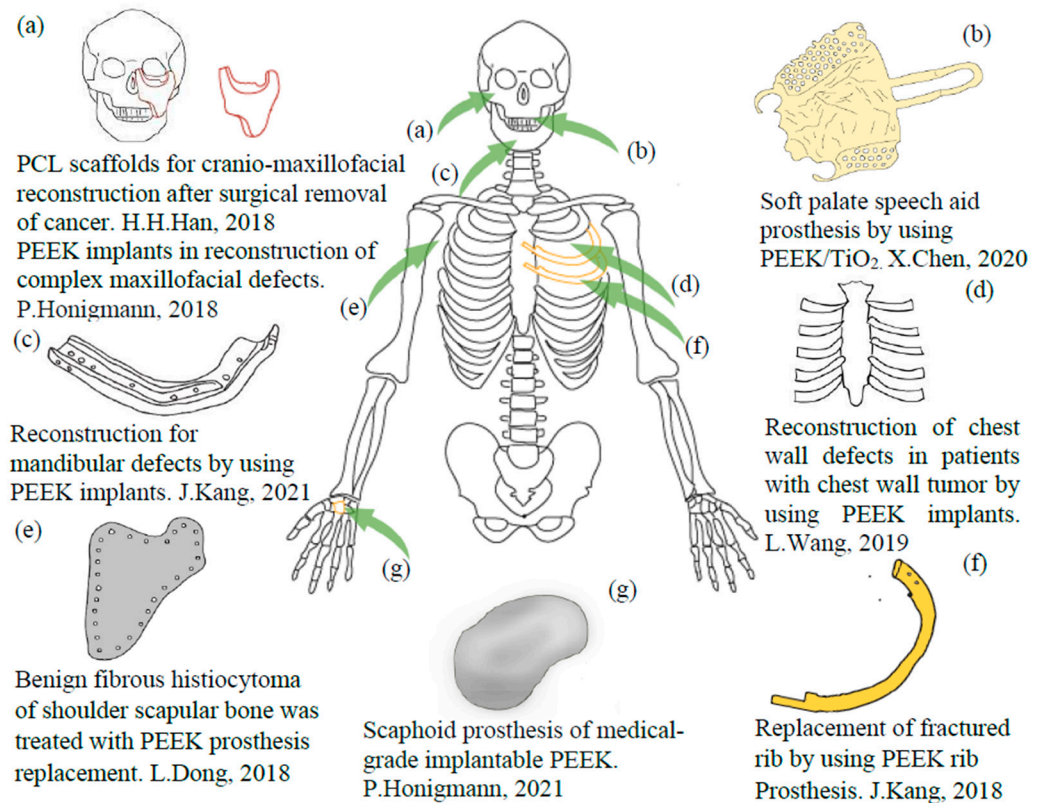


Figure 4. Summarized depiction of clinical applications reported in the studies reviewed in this paper. (For interpretation of the references to color in this figure legend, the reader is referred to the web version of this article.)

5. Conclusions

The pre-existing research on 3D-printed polymers and composites for orthopedic applications provides valuable insight into clinical applications; however, the present data are far from conclusive. Further verification can be accomplished in several ways, as follows:

- The first way is to examine high-performance materials for various medical-oriented 3D-printing techniques.
- The next approach requires using composite techniques for the production of durable polymer-based composites with superior mechanobiological performance.
- Another method involves developing new AM technologies that enable the fabrication of a complex structure with a controlled microarchitecture with high dimensional precision.
- Lastly, it would be helpful to create universal standards for 3D-printed implants and scaffold fabrication and testing.

In conclusion, this review article offers fundamental information for researchers and engineers working in this field, thus opening a new step in the development of bioengineered polymer materials.

Author Contributions: Data curation, K.M.G.; writing—original draft preparation, K.M.G. and S.I.; writing—review and editing, K.M.G. and S.I.; supervision, Z.S.B. All authors have read and agreed to the published version of the manuscript.

Funding: This research received no external funding.

Institutional Review Board Statement: Not applicable.

Informed Consent Statement: Not applicable.

Data Availability Statement: Not applicable.

Acknowledgments: We would like to acknowledge Lohit Peri Balakumar for his contributions towards the paper.

Conflicts of Interest: The authors declare no conflict of interest.

References

1. Laurencin, C.T.; Ambrosio, A.M.A.; Borden, M.D.; Cooper, J.A. Tissue engineering: Orthopedic applications. *Annu. Rev. Biomed. Eng.* **1999**, *19*, 46. [[CrossRef](#)] [[PubMed](#)]
2. Woolf, A.D.; Pfleger, B. Burden of major musculoskeletal conditions.pdf. *Bull. World Health Organ.* **2003**, *81*, 646–656. [[PubMed](#)]
3. Navarro, M.; Michiardi, A.; Castano, O.; Planell, J.A. Biomaterials in Orthopaedics. *J. R. Soc. Interface* **2008**, *5*, 1137–1158. [[CrossRef](#)]
4. Johnell, O.; Cooper, C.; Cummings, S.; Slemenda, C.; Seeman, E. The socioeconomic burden of fractures: Today and in the 21st century. *Am. J. Med.* **1997**, *103*, S20–S26. [[CrossRef](#)]
5. Kay, H.F.; Sathiyakumar, V.; Yoneda, Z.T.; Lee, Y.M.; Jahangir, A.A.; Ehrenfeld, J.M.; Obrebsky, W.T.; Apfeld, J.C.; Sethi, M.K. The effects of American society of anesthesiologists physical status on length of stay and inpatient cost in the surgical treatment of isolated orthopaedic fractures. *J. Orthop. Trauma* **2014**, *28*, 153–159. [[CrossRef](#)]
6. Yan, Q.; Dong, H.; Su, J.; Han, J.; Song, B.; Wei, Q.; Shi, Y. A Review of 3D Printing Technology for Medical Applications. *Engineering* **2018**, *4*, 729–742. [[CrossRef](#)]
7. Harsini, S.M.; Oryan, A. Bone Grafting and the Materials for Using in Orthopedics. *EC Orthop.* **2018**, *9*, 822–833.
8. Qin, C.; Lu, T.; Yang, B.; Wang, R. Xenotransplantation: Current Status in Preclinical Research. *Front. Immunol.* **2020**, *1*, 3060. [[CrossRef](#)]
9. Mitsuo, N.; Narushima, T.; Nakai, M. *Advances in Metallic Biomaterials: Tissues, Materials and Biological Reactions*; Springer: Berlin/Heidelberg, Germany, 2015. [[CrossRef](#)]
10. Walley, K.C.; Bajraliu, M.; Gonzalez, T.; Nazarian, A. The Chronicle of a Stainless Steel Orthopaedic Implant. *Orthop. J. Harvard Med. Sch.* **2016**, *17*, 68–74.
11. Kanchanomai, C.; Phiphobmongkol, V.; Muanjan, P. Fatigue failure of an orthopedic implant—A locking compression plate. *Eng. Fail. Anal.* **2008**, *15*, 521–530. [[CrossRef](#)]
12. Patel, B.; Favaro, G.; Inam, F.; Reece, M.J.; Angadji, A.; Bonfield, W.; Huang, J.; Edirisinghe, M. Cobalt-based orthopaedic alloys: Relationship between forming route, microstructure and tribological performance. *Mater. Sci. Eng. C* **2012**, *32*, 1222–1229. [[CrossRef](#)]
13. Limmahakhun, S.; Oloyede, A.; Chantarapanich, N.; Jiamwatthanachai, P.; Sitthiseripratip, K.; Xiao, Y.; Yan, C. Alternative designs of load-sharing cobalt chromium graded femoral stems. *Mater. Today Commun.* **2017**, *12*, 1–10. [[CrossRef](#)]
14. Geetha, M.; Singh, A.K.; Asokamani, R.; Gogia, A.K. Ti based biomaterials, the ultimate choice for orthopaedic implants—A review. *Prog. Mater. Sci.* **2009**, *54*, 397–425. [[CrossRef](#)]
15. Lewallen, E.A.; Riester, S.M.; Bonin, C.A.; Kremers, H.M.; Dudakovic, A.; Kakar, S.; Cohen, R.C.; Westendorf, J.J.; Lewallen, D.G.; Van Wijnen, A.J. Biological strategies for improved osseointegration and osteoinduction of porous metal orthopedic implants. *Tissue Eng. Part B Rev.* **2015**, *21*, 218–230. [[CrossRef](#)] [[PubMed](#)]
16. Semlitsch, M.F.; Weber, H.; Streicher, R.M.; Schön, R. Joint replacement components made of hot-forged and surface-treated Ti-6Al-7Nb alloy. *Biomaterials* **1992**, *13*, 781–788. [[CrossRef](#)]
17. Vendittoli, P.A.; Mottard, S.; Roy, A.G.; Dupont, C.; Lavigne, M. Chromium and cobalt ion release following the Durom high carbon content, forged metal-on metal surface replacement of the hip. *J. Bone Jt. Surg. Ser. B* **2007**, *89*, 441–448. [[CrossRef](#)] [[PubMed](#)]
18. Jaiswal, S.; Agrawal, S.; Dubey, A.; Lahiri, D. Effect of multi-axial hot forging process on mechanical, and corrosion resistance behavior of Mg-3Zn alloy for temporary orthopedic implants. *Eng. Rep.* **2020**, *3*, e12286.
19. Harris, K.; Sikkenga, S. Investment Cast Cobalt Alloys. *Cobalt News* **1999**, *4*, 3–7.
20. Babaie, E.; Bhaduri, S.B. Fabrication Aspects of porous biomaterials in orthopedic applications: A Review. *ACS Biomater. Sci. Eng.* **2018**, *4*, 1–39. [[CrossRef](#)]
21. Han, X.; Yang, D.; Yang, C.; Spintzyk, S.; Scheideler, L.; Li, P.; Li, D.; Geis-Gerstorf, J.; Rupp, F. Carbon Fiber Reinforced PEEK Composites Based on 3D-Printing Technology for Orthopedic and Dental Applications. *J. Clin. Med.* **2019**, *8*, 240. [[CrossRef](#)]

22. Ridzwan, M.I.Z.; Shuib, S.; Hassan, A.Y.; Shokri, A.A.; Mohammad Ibrahim, M.N. Problem of stress shielding and improvement to the hip implant designs: A review. *J. Med. Sci.* **2007**, *7*, 460–467. [[CrossRef](#)]
23. Sumner, D.R. Long-term implant fixation and stress-shielding in total hip replacement. *J. Biomech.* **2015**, *48*, 797–800. [[CrossRef](#)]
24. Sedel, L. Evolution of Alumina-on-Alumina Implants. *Clin. Orthop. Relat. Res.* **2000**, *379*, 48–54. [[CrossRef](#)]
25. D'Antonio, J.; Capello, W.; Manley, M.; Bierbaum, B. New experience with alumina-on-alumina ceramic bearings for total hip arthroplasty. *J. Arthroplasty* **2002**, *17*, 390–397. [[CrossRef](#)]
26. LeGeros, R.Z. Calcium phosphate-based osteoinductive materials. *Chem. Rev.* **2008**, *108*, 4742–4753. [[CrossRef](#)]
27. Daculsi, G.; Laboux, O.; Malard, O.; Weiss, P. Current Current state of the art of biphasic calcium phosphate bioceramics. *J. Mater. Sci. Mater. Med.* **2003**, *14*, 195–200. [[CrossRef](#)]
28. Clarke, I.C.; Manaka, M.; Green, D.D.; Williams, P.; Pezzotti, G.; Kim, Y.H.; Ries, M.; Sugano, N.; Sedel, L.; Delauney, C.; et al. Current status of zirconia used in total hip implants. *J. Bone Jt. Surg. Ser. A* **2003**, *85*, 73–84. [[CrossRef](#)]
29. Kohal, R.J.; Bächle, M.; Att, W.; Chaar, S.; Altmann, B.; Renz, A.; Butz, F. Osteoblast and bone tissue response to surface modified zirconia and titanium implant materials. *Dent. Mater.* **2013**, *29*, 763–776. [[CrossRef](#)]
30. Arita, M.; Takahashi, Y.; Pezzotti, G.; Shishido, T.; Masaoka, T.; Sano, K.; Yamamoto, K. Environmental Stability and Residual Stresses in Zirconia Femoral Head for Total Hip Arthroplasty: In Vitro Aging versus Retrieval Studies. *Biomed Res. Int.* **2015**, *2015*, 638502. [[CrossRef](#)]
31. Rizwan, M.; Hamdi, M.; Basirun, W.J. Bioglass@45S5-based composites for bone tissue engineering and functional applications. *J. Biomed. Mater. Res. Part A* **2017**, *105*, 3197–3223. [[CrossRef](#)]
32. Ma, R.; Tang, T. Current strategies to improve the bioactivity of PEEK. *Int. J. Mol. Sci.* **2014**, *15*, 5426–5445. [[CrossRef](#)]
33. Senra, M.R.; Marques, M.D.F.V. Synthetic Polymeric Materials for Bone Replacement. *J. Compos. Sci.* **2020**, *4*, 191. [[CrossRef](#)]
34. Tappa, K.; Jammalamadaka, U. Novel biomaterials used in medical 3D printing techniques. *J. Funct. Biomater.* **2018**, *9*, 17. [[CrossRef](#)]
35. D'Alessio, J.; Christensen, A. *3D Printing for Commercial Orthopedic Applications*; Elsevier Inc.: Amsterdam, The Netherlands, 2019. [[CrossRef](#)]
36. Bourell, D.; Espalin, D.; Arcaute, K.; Rodriguez, D.; Medina, F.; Posner, M.; Wicker, R. Fused deposition modeling of patient specific polymethylmethacrylate implants. *Rapid Prototyp. J.* **2010**, *16*, 164–173. [[CrossRef](#)]
37. Yarimitsu, S.; Sasaki, S.; Murakami, T.; Suzuki, A. Evaluation of lubrication properties of hydrogel artificial cartilage materials for joint prosthesis. *Biosurf. Biotribol.* **2016**, *2*, 40–47. [[CrossRef](#)]
38. Han, H.H.; Shim, J.H.; Lee, H.; Kim, B.Y.; Lee, J.S.; Jung, J.W.; Yun, W.S.; Baek, C.H.; Rhie, J.W.; Cho, D.W. Reconstruction of complex maxillary defects using patient-specific 3D-printed biodegradable scaffolds. *Plast. Reconstr. Surg. Glob. Open* **2018**, *6*, e1975. [[CrossRef](#)] [[PubMed](#)]
39. Singh, S.; Prakash, C.; Ramakrishna, S. 3D printing of polyether-ether-ketone for biomedical applications. *Eur. Polym. J.* **2019**, *114*, 234–248. [[CrossRef](#)]
40. Wang, Y.; Müller, W.; Rumjahn, A.; Schmidt, F.; Schwitalla, D. Mechanical properties of fused filament fabricated PEEK for biomedical applications depending on additive manufacturing parameters. *J. Mech. Behav. Biomed. Mater.* **2021**, *115*, 104250. [[CrossRef](#)]
41. Wang, L.; Huang, L.; Li, X.; Zhong, D.; Li, D. Three-Dimensional Printing PEEK Implant: A Novel Choice for the Reconstruction of Chest Wall Defect. *Ann. Thorac. Surg.* **2019**, *107*, 921–928. [[CrossRef](#)]
42. Kim, S.E.; Yun, Y.P.; Shim, K.S.; Kim, H.J.; Park, K.; Song, H.R. 3D printed alendronate-releasing poly(caprolactone) porous scaffolds enhance osteogenic differentiation and bone formation in rat tibial defects. *Biomed. Mater.* **2016**, *11*, 055005. [[CrossRef](#)]
43. Zhang, Z.Z.; Wang, S.J.; Zhang, J.Y.; Jiang, W.B.; Huang, A.B.; Qi, Y.S.; Ding, J.X.; Chen, X.S.; Jiang, D.; Yu, J.K. 3D-Printed Poly(ϵ -caprolactone) Scaffold Augmented with Mesenchymal Stem Cells for Total Meniscal Substitution: A 12- and 24-Week Animal Study in a Rabbit Model. *Am. J. Sports Med.* **2017**, *45*, 1497–1511. [[CrossRef](#)] [[PubMed](#)]
44. Brach del Prever, E.M.; Bistolfi, A.; Bracco, P.; Costa, L. UHMWPE for arthroplasty: Past or future? *J. Orthop. Traumatol.* **2009**, *10*, 1–8. [[CrossRef](#)] [[PubMed](#)]
45. Saito, N.; Aoki, K.; Usui, Y.; Shimizu, M.; Hara, K.; Narita, N.; Ogihara, N.; Nakamura, K.; Ishigaki, N.; Kato, H.; et al. Application of carbon fibers to biomaterials: A new era of nano-level control of carbon fibers after 30-years of development. *Chem. Soc. Rev.* **2011**, *40*, 3824–3834. [[CrossRef](#)] [[PubMed](#)]
46. Ramakrishna, S.; Mayer, J.; Wintermantel, E.; Leong, K. Biomedical applications of polymer-composite material: A review. *Compos. Sci. Technol.* **2001**, *61*, 1189–1224. [[CrossRef](#)]
47. Cheung, H.Y.; Lau, K.T.; Lu, T.P.; Hui, D. A critical review on polymer-based bio-engineered materials for scaffold development. *Compos. Part B Eng.* **2007**, *38*, 291–300. [[CrossRef](#)]
48. Katti, K.S.; Verma, D.; Katti, D.R. *Materials for Joint Replacement*; Elsevier: Amsterdam, The Netherlands, 2008; pp. 81–104. [[CrossRef](#)]
49. Liu, H.; Webster, T.J. Bioinspired Nanocomposites for Orthopedic Applications. In *Nanotechnology for the Regeneration of Hard and Soft Tissues*; World Scientific: Singapore, 2007. [[CrossRef](#)]
50. Steinberg, E.L.; Rath, E.; Shlaifer, A.; Chechik, O.; Maman, E.; Salai, M. Carbon fiber reinforced PEEK Optima-A composite material biomechanical properties and wear/debris characteristics of CF-PEEK composites for orthopedic trauma implants. *J. Mech. Behav. Biomed. Mater.* **2013**, *17*, 221–228. [[CrossRef](#)]

51. Ghanbari, A.; Kargar, S. Preparation of Ni-P-Al₂O₃-TiO₂ Nano composite coating by Electroless. In Proceedings of the 7th International Conference on Nanostructures (ICNS7), Tehran, Iran, 27 February–1 March 2018; p. ADV-41.
52. Kargar, S.; Ghanbari, A.; Moosavi, A.; Seyedraoufi, Z. Simulation of Flow Ni-P-Al₂O₃-TiO₂ nano composite coating by Prediction (ANN). In Proceedings of the 7th International Conference on Nanostructures (ICNS7), Tehran, Iran, 27 February–1 March 2018; p. BLK-19.
53. Chen, X.; Gao, C.; Jiang, J.; Wu, Y.; Zhu, P.; Chen, G. 3D printed porous PLA/nHA composite scaffolds with enhanced osteogenesis and osteoconductivity in vivo for bone regeneration. *Biomed. Mater.* **2019**, *14*, 065003. [[CrossRef](#)]
54. Tanodekaew, S.; Channasanon, S.; Kaewkong, P.; Uppanan, P. PLA-HA scaffolds: Preparation and bioactivity. *Procedia Eng.* **2013**, *59*, 144–149. [[CrossRef](#)]
55. Jeong, S.I.; Ko, E.K.; Yum, J.; Jung, C.H.; Lee, Y.M.; Shin, H. Nanofibrous poly(lactic acid)/hydroxyapatite composite scaffolds for guided tissue regeneration. *Macromol. Biosci.* **2008**, *8*, 328–338. [[CrossRef](#)]
56. Lui, H.; Webster, T.J. Mechanical properties of dispersed ceramic nanoparticles in polymer composites for orthopedic applications. *Int. J. Nanomed.* **2010**, *5*, 299.
57. Jose, M.V.; Thomas, V.; Johnson, K.T.; Dean, D.R.; Nyairo, E. Aligned PLGA/HA nanofibrous nanocomposite scaffolds for bone tissue engineering. *Acta Biomater.* **2009**, *5*, 305–315. [[CrossRef](#)] [[PubMed](#)]
58. Kang, Y.; Scully, A.; Young, D.A.; Kim, S.; Tsao, H.; Sen, M.; Yang, Y. Enhanced mechanical performance and biological evaluation of a PLGA coated β -TCP composite scaffold for load-bearing applications. *Eur. Polym. J.* **2011**, *47*, 1569–1577. [[CrossRef](#)] [[PubMed](#)]
59. Ebrahimian-Hosseiniabadi, M.; Ashrafzadeh, F.; Etemadifar, M.; Venkatraman, S.S. Evaluating and Modeling the Mechanical Properties of the Prepared PLGA/nano-BCP Composite Scaffolds for Bone Tissue Engineering. *J. Mater. Sci. Technol.* **2011**, *27*, 1105–1112. [[CrossRef](#)]
60. Vaezi, M.; Black, C.; Gibbs, D.M.R.; Oreffo, R.O.C.; Brady, M.; Moshrefi-Torbati, M.; Yang, S. Characterization of New PEEK/HA composites with 3D HA network fabricated by extrusion freeforming. *Molecules* **2016**, *21*, 687. [[CrossRef](#)] [[PubMed](#)]
61. Vaezi, M.; Yang, S. A novel bioactive PEEK/HA composite with controlled 3D interconnected HA network. *Int. J. Bioprint.* **2015**, *1*, 66–76. [[CrossRef](#)]
62. Uddin, M.N.; Dhanasekaran, P.S.; Asmatulu, R. Mechanical properties of highly porous PEEK bionanocomposites incorporated with carbon and hydroxyapatite nanoparticles for scaffold applications. *Prog. Biomater.* **2019**, *8*, 211–221. [[CrossRef](#)]
63. Haider, A.; Haider, S.; Rao Kummara, M.; Kamal, T.; Alghyamah, A.A.A.; Jan Iftikhar, F.; Bano, B.; Khan, N.; Amjid Afridi, M.; Soo Han, S.; et al. Advances in the scaffolds fabrication techniques using biocompatible polymers and their biomedical application: A technical and statistical review. *J. Saudi Chem. Soc.* **2020**, *24*, 186–215. [[CrossRef](#)]
64. Asefnejad, A.; Mohammad, T.K.; Aliasghar, B.; Babak, F.; Shahin, B. Manufacturing of biodegradable polyurethane scaffolds based on polycaprolactone using a phase separation method: Physical properties and in vitro assay. *Int. J. Nanomed.* **2011**, *6*, 2375–2384. [[CrossRef](#)]
65. Nam, Y.S.; Park, T.G. Porous biodegradable polymeric scaffolds prepared by thermally induced phase separation. *J. Biomed. Mater. Res.* **1999**, *47*, 8–17. [[CrossRef](#)]
66. Gautam, S.; Dinda, A.K.; Mishra, N.C. Fabrication and characterization of PCL/gelatin composite nanofibrous scaffold for tissue engineering applications by electrospinning method. *Mater. Sci. Eng. C* **2013**, *33*, 1228–1235. [[CrossRef](#)]
67. Zhao, L.; He, C.; Gao, Y.; Cen, L.; Cui, L.; Cao, Y. Preparation and cytocompatibility of PLGA scaffolds with controllable fiber morphology and diameter using electrospinning method. *J. Biomed. Mater. Res. Part B Appl. Biomater.* **2008**, *87*, 26–34. [[CrossRef](#)] [[PubMed](#)]
68. Hou, Q.; Grijpma, D.W.; Feijen, J. Preparation of Interconnected Highly Porous Polymeric Structures by a Replication and Freeze-Drying Process. *J. Biomed. Mater. Res. Part B Appl. Biomater.* **2003**, *67*, 732–740. [[CrossRef](#)] [[PubMed](#)]
69. Hou, Q.; Grijpma, D.W.; Feijen, J. Porous polymeric structures for tissue engineering prepared by a coagulation, compression moulding and salt leaching technique. *Biomaterials* **2003**, *24*, 1937–1947. [[CrossRef](#)]
70. Liao, C.J.; Chen, C.F.; Chen, J.H.; Chiang, S.F.; Lin, Y.J.; Chang, K.Y. Fabrication of porous biodegradable polymer scaffolds using a solvent merging/particulate leaching method. *J. Biomed. Mater. Res.* **2002**, *59*, 676–681. [[CrossRef](#)] [[PubMed](#)]
71. Oh, S.H.; Kang, S.G.; Kim, E.S.; Cho, S.H.; Lee, J.H. Fabrication and characterization of hydrophilic poly(lactic-co-glycolic acid)/poly(vinyl alcohol) blend cell scaffolds by melt-molding particulate-leaching method. *Biomaterials* **2003**, *24*, 4011–4021. [[CrossRef](#)]
72. Young, M.J.; Park, K.; Jun, S.S.; Kim, J.J.; Rhie, J.W.; Han, D.K. Beneficial effect of hydrophilized porous polymer scaffolds in tissue-engineered cartilage formation. *J. Biomed. Mater. Res. Part B Appl. Biomater.* **2008**, *85*, 252–260. [[CrossRef](#)]
73. Moghadam, M.Z.; Hassanajili, S.; Esmaeilzadeh, F.; Ayatollahi, M.; Ahmadi, M. Formation of porous HPCL/LPCL/HA scaffolds with supercritical CO₂ gas foaming method. *J. Mech. Behav. Biomed. Mater.* **2017**, *69*, 115–127. [[CrossRef](#)] [[PubMed](#)]
74. Lyons, R.; Newell, A.; Ghadimi, P.; Papakostas, N. Environmental impacts of conventional and additive manufacturing for the production of Ti-6Al-4V knee implant: A life cycle approach. *Int. J. Adv. Manuf. Technol.* **2020**, *112*, 787–801. [[CrossRef](#)]
75. Cronskär, M.; Bäckström, M.; Rännar, L.E. Production of customized hip stem prostheses - A comparison between conventional machining and electron beam melting (EBM). *Rapid Prototyp. J.* **2013**, *19*, 365–372. [[CrossRef](#)]
76. Costantini, M.; Barbetta, A. *Gas Foaming Technologies for 3D scaffold Engineering*; Elsevier Ltd.: Amsterdam, The Netherlands, 2018. [[CrossRef](#)]

77. Boudriot, U.; Dersch, R.; Greiner, A.; Wendorff, J.H. Electrospinning approaches toward scaffold engineering—A brief overview. *Artif. Organs* **2006**, *30*, 785–792. [[CrossRef](#)]
78. Bagaria, V.; Bhansali, R.; Pawar, P. 3D printing- creating a blueprint for the future of orthopedics: Current concept review and the road ahead! *J. Clin. Orthop. Trauma* **2018**, *9*, 207–212. [[CrossRef](#)] [[PubMed](#)]
79. Zhang, B.; Wang, L.; Song, P.; Pei, X.; Sun, H.; Wu, L.; Zhou, C.; Wang, K.; Fan, Y.; Zhang, X. 3D printed bone tissue regenerative PLA/HA scaffolds with comprehensive performance optimizations. *Mater. Des.* **2021**, *201*, 109490. [[CrossRef](#)]
80. Fan, D.; Li, Y.; Wang, X.; Zhu, T.; Wang, Q.; Cai, H.; Li, W.; Tian, Y.; Liu, Z. Progressive 3D Printing Technology and Its Application in Medical Materials. *Front. Pharmacol.* **2020**, *11*, 122. [[CrossRef](#)] [[PubMed](#)]
81. Du, W.; Ren, X.; Pei, Z.; Ma, C. Ceramic Binder Jetting Additive Manufacturing: A Literature Review on Density. *J. Manuf. Sci. Eng. Trans. ASME* **2020**, *142*, 040801. [[CrossRef](#)]
82. Zhou, Z.; Lennon, A.; Buchanan, F.; McCarthy, H.O.; Dunne, N. Binder jetting additive manufacturing of hydroxyapatite powders: Effects of adhesives on geometrical accuracy and green compressive strength. *Addit. Manuf.* **2020**, *36*, 101645. [[CrossRef](#)]
83. Szymczyk-Ziółkowska, P.; Łabowska, M.B.; Detyna, J.; Michalak, I.; Gruber, P. A review of fabrication polymer scaffolds for biomedical applications using additive manufacturing techniques. *Biocybern. Biomed. Eng.* **2020**, *40*, 624–638. [[CrossRef](#)]
84. Abdulhameed, O.; Al-Ahmari, A.; Ameen, W.; Mian, S.H. Additive manufacturing: Challenges, trends, and applications. *Adv. Mech. Eng.* **2019**, *11*, 1–27. [[CrossRef](#)]
85. Kumar, M.B.; Sathiya, P. Methods and materials for additive manufacturing: A critical review on advancements and challenges. *Thin-Walled Struct.* **2021**, *159*, 107228. [[CrossRef](#)]
86. Jared, B.H.; Aguilo, M.A.; Beghini, L.L.; Boyce, B.L.; Clark, B.W.; Cook, A.; Kaehr, B.J.; Robbins, J. Additive manufacturing: Toward holistic design. *Scr. Mater.* **2017**, *135*, 141–147. [[CrossRef](#)]
87. Guessasma, S.; Zhang, W.; Zhu, J.; Belhabib, S.; Nouri, H. Challenges of additive manufacturing technologies from an optimisation perspective. *Int. J. Simul. Multidiscip. Des. Optim.* **2015**, *6*, A9. [[CrossRef](#)]
88. Somireddy, M. Fabrication of Composite Structures via 3D Printing. In *Fused Deposition Modeling Based 3D Printing*; Springer: Berlin/Heidelberg, Germany, 2021; pp. 255–276. [[CrossRef](#)]
89. Melancon, D.; Bagheri, Z.S.; Johnston, R.B.; Liu, L.; Tanzer, M.; Pasini, D. Mechanical characterization of structurally porous biomaterials built via additive manufacturing: Experiments, predictive models, and design maps for load-bearing bone replacement implants. *Acta Biomater.* **2017**, *63*, 350–368. [[CrossRef](#)] [[PubMed](#)]
90. Bagheri, Z.S.; Melancon, D.; Liu, L.; Johnston, R.B.; Pasini, D. Compensation strategy to reduce geometry and mechanics mismatches in porous biomaterials built with Selective Laser Melting. *J. Mech. Behav. Biomed. Mater.* **2017**, *70*, 17–27. [[CrossRef](#)] [[PubMed](#)]
91. Piat, R.; Sinchuk, Y.; Vasoya, M.; Sigmund, O. Minimal compliance design for metal-ceramic composites with lamellar microstructures. *Acta Mater.* **2011**, *59*, 4835–4846. [[CrossRef](#)]
92. Kum, S.G.; Laurencin, C.; Deng, M. *Natural and Synthetic Biomedical Polymers*; Elsevier Science & Technology: Saint Louis, MI, USA, 2014.
93. Allan, B.; Ruan, R.; Landao-Bassonga, E.; Gillman, N.; Wang, T.; Gao, J.; Ruan, Y.; Xu, Y.; Lee, C.; Goonewardene, M.; et al. Collagen membrane for guided bone regeneration in dental and orthopedic applications. *Tissue Eng. Part A* **2021**, *27*, 372–381. [[CrossRef](#)]
94. Cunniffe, G.M.; O'Brien, F.J. Collagen scaffolds for orthopedic regenerative medicine. *JOM* **2011**, *63*, 66–73. [[CrossRef](#)]
95. Alghamdi, H.S.; Bosco, R.; van den Beucken, J.J.J.P.; Walboomers, X.F.; Jansen, J.A. Osteogenicity of titanium implants coated with calcium phosphate or collagen type-I in osteoporotic rats. *Biomaterials* **2013**, *34*, 3747–3757. [[CrossRef](#)]
96. Lee, Y.H.; Lee, B.W.; Jung, Y.C.; Yoon, B.I.; Woo, H.M.; Kang, B.J. Application of alginate microbeads as a carrier of bone morphogenetic protein-2 for bone regeneration. *J. Biomed. Mater. Res. Part B Appl. Biomater.* **2019**, *107*, 286–294. [[CrossRef](#)]
97. Chen, Q.; Cordero-Arias, L.; Roether, J.A.; Cabanas-Polo, S.; Virtanen, S.; Boccaccini, A.R. Alginate/Bioglass® composite coatings on stainless steel deposited by direct current and alternating current electrophoretic deposition. *Surf. Coat. Technol.* **2013**, *233*, 49–56. [[CrossRef](#)]
98. Ho, H.V.; Tripathi, G.; Gwon, J.; Lee, S.Y.; Lee, B.T. Novel TOCNF reinforced injectable alginate β -tricalcium phosphate microspheres for bone regeneration. *Mater. Des.* **2020**, *194*, 108892. [[CrossRef](#)]
99. Arjmandi, M.; Ramezani, M.; Nand, A.; Neitzert, T. Experimental study on friction and wear properties of interpenetrating polymer network alginate-polyacrylamide hydrogels for use in minimally-invasive joint implants. *Wear* **2018**, *406–407*, 194–204. [[CrossRef](#)]
100. Varoni, E.; Tschon, M.; Palazzo, B.; Nitti, P.; Martini, L.; Rimondini, L. Agarose Gel as Biomaterial or Scaffold for Implantation Surgery: Characterization, Histological and Histomorphometric Study on Soft Tissue Response. *Connect. Tissue Res.* **2012**, *53*, 548–554. [[CrossRef](#)] [[PubMed](#)]
101. Melis Soylu, H.; Chevallier, P.; Copes, F.; Ponti, F.; Candiani, G.; Yurt, F.; Mantovani, D.; Li, Y.; Nan, K. A Novel Strategy to Coat Dopamine-Functionalized Titanium Surfaces With Agarose-Based Hydrogels for the Controlled Release of Gentamicin. *Article* **2021**, *11*, 1. [[CrossRef](#)]
102. Gupta, A.; Bhat, S.; Jagdale, P.R.; Chaudhari, B.P.; Lidgren, L.; Gupta, K.C.; Kumar, A. Evaluation of three-dimensional chitosan-agarose-gelatin cryogel scaffold for the repair of subchondral cartilage defects: An in vivo study in a rabbit model. *Tissue Eng. Part A* **2014**, *20*, 3101–3111. [[CrossRef](#)]

103. Figueiredo, L.; Fonseca, R.; Pinto, L.F.V.; Ferreira, F.C.; Almeida, A.; Rodrigues, A. Strategy to improve the mechanical properties of bioabsorbable materials based on chitosan for orthopedic fixation applications. *J. Mech. Behav. Biomed. Mater.* **2020**, *103*, 103572. [[CrossRef](#)] [[PubMed](#)]
104. Francis, A.; Yang, Y.; Boccaccini, A.R. A new strategy for developing chitosan conversion coating on magnesium substrates for orthopedic implants. *Appl. Surf. Sci.* **2019**, *466*, 854–862. [[CrossRef](#)]
105. Pighinelli, L.; Kucharska, M. Chitosan-hydroxyapatite composites. *Carbohydr. Polym.* **2013**, *93*, 256–262. [[CrossRef](#)]
106. Tuzlakoglu, K.; Reis, R.L. Introduction: Chemical and Physical Structure of Chitosan and Its. In *Woodhead Publishing Series in Biomaterials*; Woodhead Publishing: Sawston, UK, 2008; pp. 357–373. [[CrossRef](#)]
107. Qin, L.; Dong, H.; Mu, Z.; Zhang, Y.; Dong, G. Preparation and bioactive properties of chitosan and casein phosphopeptides composite coatings for orthopedic implants. *Carbohydr. Polym.* **2015**, *133*, 236–244. [[CrossRef](#)] [[PubMed](#)]
108. Ahmed, R.A.; Fekry, A.M.; Farghali, R.A. A study of calcium carbonate/multiwalled-carbon nanotubes/chitosan composite coatings on Ti-6Al-4V alloy for orthopedic implants. *Appl. Surf. Sci.* **2013**, *285*, 309–316. [[CrossRef](#)]
109. Deepachitra, R.; Nigam, R.; Purohit, S.D.; Kumar, B.S.; Hemalatha, T.; Sastry, T.P. In Vitro Study of Hydroxyapatite Coatings on Fibrin Functionalized/Pristine Graphene Oxide for Bone Grafting. *Mater. Manuf. Process.* **2015**, *30*, 804–811. [[CrossRef](#)]
110. Noori, A.; Ashrafi, S.J.; Vaez-Ghaemi, R.; Hatamian-Zaremi, A.; Webster, T.J. A review of fibrin and fibrin composites for bone tissue engineering. *Int. J. Nanomed.* **2017**, *12*, 4937. [[CrossRef](#)]
111. Kobayashi, M.; Hyu, H.S. Development and Evaluation of Polyvinyl Alcohol-Hydrogels as an Artificial Articular Cartilage for Orthopedic Implants. *Materials (Basel)* **2010**, *3*, 2753–2771. [[CrossRef](#)]
112. Pitarresi, G.; Palumbo, F.S.; Calascibetta, F.; Fiorica, C.; Di Stefano, M.; Giammona, G. Medicated hydrogels of hyaluronic acid derivatives for use in orthopedic field. *Int. J. Pharm.* **2013**, *449*, 84–94. [[CrossRef](#)] [[PubMed](#)]
113. Zhai, P.; Peng, X.; Li, B.; Liu, Y.; Sun, H.; Li, X. The application of hyaluronic acid in bone regeneration. *Int. J. Biol. Macromol.* **2020**, *151*, 1224–1239. [[CrossRef](#)] [[PubMed](#)]
114. Martínez-Sanz, E.; Ossipov, D.A.; Hilborn, J.; Larsson, S.; Jonsson, K.B.; Varghese, O.P. Bone reservoir: Injectable hyaluronic acid hydrogel for minimal invasive bone augmentation. *J. Control. Release* **2011**, *152*, 232–240. [[CrossRef](#)]
115. Peppas, N.A.; Hoffman, A.S. Hydrogels. *Elsevier* **2020**, 153–166. [[CrossRef](#)]
116. Maitz, M.F. Applications of synthetic polymers in clinical medicine. *Biosurf. Biotribol.* **2015**, *1*, 161–176. [[CrossRef](#)]
117. Velu, R.; Calais, T.; Jayakumar, A.; Raspall, F. A comprehensive review on bio-nanomaterials for medical implants and feasibility studies on fabrication of such implants by additive manufacturing technique. *Materials* **2020**, *13*, 92. [[CrossRef](#)]
118. Yao, C.H.; Lai, Y.H.; Chen, Y.W.; Cheng, C.H. Bone Morphogenetic Protein-2-Activated 3D-Printed Poly(lactic acid) Scaffolds to Promote Bone Regrowth and Repair. *Macromol. Biosci.* **2020**, *20*, 1–15. [[CrossRef](#)]
119. Singhvi, M.S.; Zinjarde, S.S.; Gokhale, D.V. Poly(lactic acid): Synthesis and biomedical applications. *J. Appl. Microbiol.* **2019**, *127*, 1612–1626. [[CrossRef](#)]
120. Burge, G.; Aytac, E.; Evcil, A.; Savas, M.A. An Investigation on Mechanical Properties of PLA Produced by 3D Printing as an Implant Material. In Proceedings of the 2020 4th International Symposium on Multidisciplinary Studies and Innovative Technologies (ISMSIT), Istanbul, Turkey, 22–24 October 2020. [[CrossRef](#)]
121. Chen, X.; Chen, G.; Wang, G.; Zhu, P.; Gao, C. Recent Progress on 3D-Printed Poly(lactic acid) and Its Applications in Bone Repair. *Adv. Eng. Mater.* **2020**, *22*, 1–19. [[CrossRef](#)]
122. Wu, C.; Wang, S.; Wu, D.; Shih, W. Novel composite 3D-printed filament made from fish scale-derived hydroxyapatite, eggshell and poly(lactic acid) via a fused fabrication approach. *Addit. Manuf.* **2021**, *46*, 102169. [[CrossRef](#)]
123. Alksne, M.; Kalvaityte, M.; Simoliunas, E.; Rinkunaite, I.; Gendviliene, I.; Locs, J.; Rutkunas, V.; Bukelskiene, V. In vitro comparison of 3D printed poly(lactic acid)/hydroxyapatite and poly(lactic acid)/bioglass composite scaffolds: Insights into materials for bone regeneration. *J. Mech. Behav. Biomed. Mater.* **2020**, *104*, 103641. [[CrossRef](#)] [[PubMed](#)]
124. Nazeer, M.A.; Onder, O.C.; Sevgili, I.; Yilgor, E.; Kavakli, I.H.; Yilgor, I. 3D printed poly(lactic acid) scaffolds modified with chitosan and hydroxyapatite for bone repair applications. *Mater. Today Commun.* **2020**, *25*, 101515. [[CrossRef](#)]
125. Luo, Y.; Humayun, A.; Mills, D.K. Surface Modification of 3D Printed PLA / Halloysite Composite Scaffolds with Antibacterial and Osteogenic Capabilities. *Appl. Sci.* **2020**, *10*, 3971. [[CrossRef](#)]
126. Singh, D.; Babbar, A.; Jain, V.; Gupta, D.; Saxena, S.; Dwivedi, V. Synthesis, characterization, and bioactivity investigation of biomimetic biodegradable PLA scaffold fabricated by fused filament fabrication process. *J. Brazilian Soc. Mech. Sci. Eng.* **2019**, *41*, 1–13. [[CrossRef](#)]
127. Wang, P.; Yin, H.M.; Li, X.; Liu, W.; Chu, Y.X.; Wang, Y.; Wang, Y.; Xu, J.Z.; Li, Z.M.; Li, J.H. Simultaneously constructing nanotopographical and chemical cues in 3D-printed poly(lactic acid) scaffolds to promote bone regeneration. *Mater. Sci. Eng. C* **2021**, *118*, 111457. [[CrossRef](#)] [[PubMed](#)]
128. Wang, M.; Favi, P.; Cheng, X.; Golshan, N.H.; Ziemer, K.S.; Keidar, M.; Webster, T.J. Cold atmospheric plasma (CAP) surface nanomodified 3D printed poly(lactic acid) (PLA) scaffolds for bone regeneration. *Acta Biomater.* **2016**, *46*, 256–265. [[CrossRef](#)]
129. Dubinenko, G.E.; Zinoviev, A.L.; Bolbasov, E.N.; Novikov, V.T.; Tverdokhlebov, S.I. Preparation of Poly(L-lactic acid)/Hydroxyapatite composite scaffolds by fused deposit modeling 3D printing. *Mater. Today Proc.* **2020**, *22*, 228–234. [[CrossRef](#)]
130. Omigbodun, F.T.; Engstrom, D.S.; Mele, E. Improving Mechanical strength of bone-implant with primitive and gyroid lattice of PLA/cHAP and rGO composites. *J. Hazard. Mater.* **2020**, 124370. [[CrossRef](#)]

131. Sahmani, S.; Khandan, A.; Saber-Samandari, S.; Esmaeili, S.; Aghdam, M.M. Fabrication and resonance simulation of 3D-printed biocomposite mesoporous implants with different periodic cellular topologies. *Bioprinting* **2021**, *22*, e00138. [[CrossRef](#)]
132. Elhattab, K.; Bhaduri, S.B.; Lawrence, J.G.; Sikder, P. Fused Filament Fabrication (Three-Dimensional Printing) of Amorphous Magnesium Phosphate/Poly(lactic acid) Macroporous Biocomposite Scaffolds. *ACS Appl. Bio Mater.* **2021**, *4*, 3276–3286. [[CrossRef](#)] [[PubMed](#)]
133. Ranjan, N.; Singh, R.; Ahuja, I.P.S.; Kumar, R.; Singh, J.; Verma, A.K.; Leekha, A. On 3D printed scaffolds for orthopedic tissue engineering applications. *SN Appl. Sci.* **2020**, *2*, 192. [[CrossRef](#)]
134. Tcacencu, I.; Rodrigues, N.; Alharbi, N.; Benning, M.; Toumpaniari, S.; Mancuso, E.; Marshall, M.; Bretcanu, O.; Birch, M.; McCaskie, A.; et al. Osseointegration of porous apatite-wollastonite and poly(lactic acid) composite structures created using 3D printing techniques. *Mater. Sci. Eng. C* **2018**, *90*, 1–7. [[CrossRef](#)] [[PubMed](#)]
135. Zhang, H.; Mao, X.; Zhao, D.; Jiang, W.; Du, Z.; Li, Q.; Jiang, C.; Han, D. Three dimensional printed polylactic acid-hydroxyapatite composite scaffolds for prefabricating vascularized tissue engineered bone: An in vivo bioreactor model. *Sci. Rep.* **2017**, *7*, 15255. [[CrossRef](#)]
136. Liu, Z.; Ge, Y.; Zhang, L.; Wang, Y.; Guo, C.; Feng, K.; Yang, S.; Zhai, Z.; Chi, Y.; Zhao, J.; et al. The effect of induced membranes combined with enhanced bone marrow and 3D PLA-HA on repairing long bone defects in vivo. *J. Tissue Eng. Regen. Med.* **2020**, *14*, 1403–1414. [[CrossRef](#)]
137. Shen, J.; Wang, W.; Zhai, X.; Chen, B.; Qiao, W.; Li, W.; Li, P.; Zhao, Y.; Meng, Y.; Qian, S.; et al. 3D-printed nanocomposite scaffolds with tunable magnesium ionic microenvironment induce in situ bone tissue regeneration. *Appl. Mater. Today* **2019**, *16*, 493–507. [[CrossRef](#)]
138. Haverová, L.; Oriňaková, R.; Oriňak, A.; Gorejová, R.; Baláž, M.; Vanýsek, P.; Kupková, M.; Hrubovčáková, M.; Mudroň, P.; Radoňák, J.; et al. An in vitro corrosion study of open cell Iron structures with PEG coating for bone replacement applications. *Metals (Basel)* **2018**, *8*, 499. [[CrossRef](#)]
139. Luo, Y.; Pan, H.; Jiang, J.; Zhao, C.; Zhang, J.; Chen, P.; Lin, X.; Fan, S. Desktop-Stereolithography 3D Printing of a Polyporous Extracellular Matrix Bioink for Bone Defect Regeneration. *Front. Bioeng. Biotechnol.* **2020**, *8*, 1–13. [[CrossRef](#)]
140. Zhou, X.; Esworthy, T.; Lee, S.J.; Miao, S.; Cui, H.; Plesiniak, M.; Fenniri, H.; Webster, T.; Rao, R.D.; Zhang, L.G. 3D Printed scaffolds with hierarchical biomimetic structure for osteochondral regeneration. *Nanomed. Nanotechnol. Biol. Med.* **2019**, *19*, 58–70. [[CrossRef](#)]
141. Zhou, X.; Castro, N.J.; Zhu, W.; Cui, H.; Aliabouzar, M.; Sarkar, K.; Zhang, L.G. Improved Human Bone Marrow Mesenchymal Stem Cell Osteogenesis in 3D Bioprinted Tissue Scaffolds with Low Intensity Pulsed Ultrasound Stimulation. *Sci. Rep.* **2016**, *6*, 32876. [[CrossRef](#)]
142. Zhu, S.; Chen, P.; Chen, Y.; Li, M.; Chen, C.; Lu, H. 3D-Printed Extracellular Matrix/Polyethylene Glycol Diacrylate Hydrogel Incorporating the Anti-inflammatory Phytomolecule Honokiol for Regeneration of Osteochondral Defects. *Am. J. Sports Med.* **2020**, *48*, 2808–2818. [[CrossRef](#)] [[PubMed](#)]
143. Bai, J.; Wang, H.; Gao, W.; Liang, F.; Wang, Z.; Zhou, Y.; Lan, X.; Chen, X.; Cai, N.; Huang, W.; et al. Melt electrohydrodynamic 3D printed poly(ϵ -caprolactone)/polyethylene glycol/roxithromycin scaffold as a potential anti-infective implant in bone repair. *Int. J. Pharm.* **2020**, *576*, 118941. [[CrossRef](#)] [[PubMed](#)]
144. Liu, F.; Kang, H.; Liu, Z.; Jin, S.; Yan, G.; Sun, Y.; Li, F.; Zhan, H.; Gu, Y. 3D Printed Multi-Functional Scaffolds Based on Poly(ϵ -Caprolactone) and Hydroxyapatite Composites. *Nanomaterials* **2021**, *11*, 2456. [[CrossRef](#)] [[PubMed](#)]
145. Buyuksungur, S.; Endogan Tanir, T.; Buyuksungur, A.; Bektas, E.I.; Torun Kose, G.; Yucel, D.; Beyzadeoglu, T.; Cetinkaya, E.; Yenigun, C.; Tönük, E.; et al. 3D printed poly(ϵ -caprolactone) scaffolds modified with hydroxyapatite and poly(propylene fumarate) and their effects on the healing of rabbit femur defects. *Biomater. Sci.* **2017**, *5*, 2144–2158. [[CrossRef](#)]
146. Pandiyaraj, K.N.; Ghobeira, R.; Esbah Tabaei, P.S.; Cools, P.; De Geyter, N.; Morent, R.; Deshmukh, R.R. Non-thermal plasma jet-assisted development of phosphorus-containing functional coatings on 3D-printed PCL scaffolds intended for bone tissue engineering. *J. Phys. Chem. Solids* **2021**, *154*, 110025. [[CrossRef](#)]
147. Xiong, Z.; Liu, W.; Qian, H.; Lei, T.; He, X.; Hu, Y.; Lei, P. Tantalum Nanoparticles Reinforced PCL Scaffolds Using Direct 3D Printing for Bone Tissue Engineering. *Front. Mater.* **2021**, *8*, 1–7. [[CrossRef](#)]
148. Ma, J.; Lin, L.; Zuo, Y.; Zou, Q.; Ren, X.; Li, J.; Li, Y. Modification of 3D printed PCL scaffolds by PVAc and HA to enhance cytocompatibility and osteogenesis. *RSC Adv.* **2019**, *9*, 5338–5346. [[CrossRef](#)]
149. Zhao, S.; Xie, K.; Guo, Y.; Tan, J.; Wu, J.; Yang, Y.; Fu, P.; Wang, L.; Jiang, W.; Hao, Y. Fabrication and Biological Activity of 3D-Printed Polycaprolactone/Magnesium Porous Scaffolds for Critical Size Bone Defect Repair. *ACS Biomater. Sci. Eng.* **2020**, *6*, 5120–5131. [[CrossRef](#)]
150. Radhakrishnan, S.; Nagarajan, S.; Belaid, H.; Farha, C.; Iatsunskyi, I.; Coy, E.; Soussan, L.; Huon, V.; Bares, J.; Belkacemi, K.; et al. Fabrication of 3D printed antimicrobial polycaprolactone scaffolds for tissue engineering applications. *Mater. Sci. Eng. C* **2021**, *118*, 111525. [[CrossRef](#)]
151. Abdal-hay, A.; Raveendran, N.T.; Fournier, B.; Ivanovski, S. Fabrication of biocompatible and bioabsorbable polycaprolactone/magnesium hydroxide 3D printed scaffolds: Degradation and in vitro osteoblasts interactions. *Compos. Part B Eng.* **2020**, *197*, 108158. [[CrossRef](#)]
152. Amdjadi, P.; Khoshroo, K.; Seifi, M.; Tahriri, M.; Tayebi, L. Mechanical Properties of 3D Printed reinforced Polycaprolactone Composite Scaffolds. *J. Dent. Sch. Shahid Beheshti Univ. Med. Sci.* **2018**, *38*, 7. [[CrossRef](#)]

153. Golafshan, N.; Vorndran, E.; Zaharievski, S.; Brommer, H.; Kadumudi, F.B.; Dolatshahi-Pirouz, A.; Gbureck, U.; van Weeren, R.; Castilho, M.; Malda, J. Tough magnesium phosphate-based 3D-printed implants induce bone regeneration in an equine defect model. *Biomaterials* **2020**, *261*, 120302. [[CrossRef](#)] [[PubMed](#)]
154. Xu, Y.; Peng, J.; Richards, G.; Lu, S.; Eglin, D. Optimization of electrospray fabrication of stem cell-embedded alginate-gelatin microspheres and their assembly in 3D-printed poly(ϵ -caprolactone) scaffold for cartilage tissue engineering. *J. Orthop. Transl.* **2019**, *18*, 128–141. [[CrossRef](#)]
155. Hedayati, S.K.; Behraves, A.H.; Hasannia, S.; Bagheri Saed, A.; Akhoundi, B. 3D printed PCL scaffold reinforced with continuous biodegradable fiber yarn: A study on mechanical and cell viability properties. *Polym. Test.* **2020**, *83*, 106347. [[CrossRef](#)]
156. Shim, J.H.; Won, J.Y.; Park, J.H.; Bae, J.H.; Ahn, G.; Kim, C.H.; Lim, D.H.; Cho, D.W.; Yun, W.S.; Bae, E.B.; et al. Effects of 3D-printed polycaprolactone/ β -tricalcium phosphate membranes on guided bone regeneration. *Int. J. Mol. Sci.* **2017**, *18*, 899. [[CrossRef](#)]
157. DeBaun, M.R.; Stahl, A.M.; Daoud, A.I.; Pan, C.C.; Bishop, J.A.; Gardner, M.J.; Yang, Y.P. Preclinical induced membrane model to evaluate synthetic implants for healing critical bone defects without autograft. *J. Orthop. Res.* **2019**, *37*, 60–68. [[CrossRef](#)]
158. Li, J.; Chen, M.; Wei, X.; Hao, Y.; Wang, J. Evaluation of 3D-printed polycaprolactone scaffolds coated with freeze-dried platelet-rich plasma for bone regeneration. *Materials (Basel)* **2017**, *10*, 831. [[CrossRef](#)]
159. Zhou, Z.; Yao, Q.; Li, L.; Zhang, X.; Wei, B.; Yuan, L.; Wang, L. Antimicrobial activity of 3D-printed poly(ϵ -Caprolactone) (PCL) composite scaffolds presenting vancomycin-loaded poly(lactic acid-glycolic acid) (PLGA) microspheres. *Med. Sci. Monit.* **2018**, *24*, 6934–6945. [[CrossRef](#)]
160. Park, S.; Kim, J.E.; Han, J.; Jeong, S.; Lim, J.W.; Lee, M.C.; Son, H.; Kim, H.B.; Choung, Y.H.; Seonwoo, H.; et al. 3D-Printed Poly(ϵ -Caprolactone)/Hydroxyapatite Scaffolds Modified With Alkaline Hydrolysis Enhance Osteogenesis in Vitro. *Polymers* **2021**, *13*, 257. [[CrossRef](#)]
161. Lee, S.; Choi, D.; Shim, J.H.; Nam, W. Efficacy of three-dimensionally printed polycaprolactone/beta tricalcium phosphate scaffold on mandibular reconstruction. *Sci. Rep.* **2020**, *10*, 4979. [[CrossRef](#)]
162. Nyberg, E.; Rindone, A.; Dorafshar, A.; Grayson, W.L. Comparison of 3D-Printed Poly- ϵ -Caprolactone Scaffolds Functionalized with Tricalcium Phosphate, Hydroxyapatite, Bio-Oss, or Decellularized Bone Matrix. *Tissue Eng. Part A* **2017**, *23*, 503–514. [[CrossRef](#)] [[PubMed](#)]
163. Andrew Wu, Y.H.; Chiu, Y.C.; Lin, Y.H.; Ho, C.C.; Shie, M.Y.; Chen, Y.W. 3D-Printed bioactive calcium silicate/poly- ϵ -Caprolactone bioscaffolds modified with biomimetic extracellular matrices for bone regeneration. *Int. J. Mol. Sci.* **2019**, *20*, 942. [[CrossRef](#)]
164. Knutsen, A.R.; Borkowski, S.L.; Ebramzadeh, E.; Flanagan, C.L.; Hollister, S.J.; Sangiorgio, S.N. Static and dynamic fatigue behavior of topology designed and conventional 3D printed bioresorbable PCL cervical interbody fusion devices. *J. Mech. Behav. Biomed. Mater.* **2015**, *49*, 332–342. [[CrossRef](#)] [[PubMed](#)]
165. Xu, H.; Wang, C.; Liu, C.; Li, J.; Peng, Z.; Guo, J.; Zhu, L. Stem cell-seeded 3D-printed scaffolds combined with self-assembling peptides for bone defect repair. *Tissue Eng. Part A* **2021**, *28*, 111–124. [[CrossRef](#)]
166. Kalluri, L.; Duan, Y. Advances in Dental Implantology using Nanomaterials and Allied Technology Applications. In *Advances in Dental Implantology Using Nanomaterials and Allied Technology Applications*; Chaughule, R.S., Dashaputra, R., Eds.; Springer: Berlin/Heidelberg, Germany, 2021. [[CrossRef](#)]
167. Botlhoko, O.J. Preparation Characterization and Properties of Bionanohybrids Based on Biocompatible Poly (Glycolic Acid)/Polylactide Blends and Carbon Nanotubes—Towards Orthopaedic Applications by orebotse Joseph Botlhoko. Ph.D. Thesis, University of Johannesburg, Johannesburg, South Africa, 2012.
168. Prabhu, B.; Karau, A.; Wood, A.; Dadsetan, M.; Liedtke, H.; DeWitt, T. *Orthopedic Biomaterials*; Li, B., Webster, T., Eds.; Springer: Berlin/Heidelberg, Germany, 2018.
169. Benatti, A.C.B.; Pattaro, A.F.; Rodrigues, A.A.; Xavier, M.V.; Kaasi, A.; Barbosa, M.I.R.; Jardini, A.L.; Filho, R.M.; Kharmandayan, P. Bioreabsorbable polymers for tissue engineering: PLA, PGA, and their copolymers. In *Materials for Biomedical Engineering*; Elsevier: Amsterdam, The Netherlands, 2019. [[CrossRef](#)]
170. Naseem, R.; Tzivelekis, C.; German, M.; Gentile, P.; Ferreira, A.; Dalgarno, K. Strategies for Enhancing Polyester-Based Materials for Bone Fixation Applications. *Molecules* **2021**, *26*, 992. [[CrossRef](#)] [[PubMed](#)]
171. Ødegaard, K.S.; Torgersen, J.; Elverum, C.W. Structural and biomedical properties of common additively manufactured biomaterials: A concise review. *Metals (Basel)* **2020**, *10*, 1677. [[CrossRef](#)]
172. Aragón, J.; Feoli, S.; Irusta, S.; Mendoza, G. Composite scaffold obtained by electro-hydrodynamic technique for infection prevention and treatment in bone repair. *Int. J. Pharm.* **2019**, *557*, 162–169. [[CrossRef](#)]
173. Liu, C.G.; Zeng, Y.T.; Kankala, R.K.; Zhang, S.S.; Chen, A.Z.; Wang, S. Bin Characterization and preliminary biological evaluation of 3D-printed porous scaffolds for engineering bone tissues. *Materials (Basel)* **2018**, *11*, 1832. [[CrossRef](#)]
174. Zhao, D.; Zhu, T.; Li, J.; Cui, L.; Zhang, Z.; Zhuang, X.; Ding, J. Poly(lactic-co-glycolic acid)-based composite bone-substitute materials. *Bioact. Mater.* **2021**, *6*, 346–360. [[CrossRef](#)]
175. Babilotte, J.; Martin, B.; Guduric, V.; Bareille, R.; Agniel, R.; Roques, S.; Héroguez, V.; Dussauze, M.; Gaudon, M.; Le Nihouannen, D.; et al. Development and characterization of a PLGA-HA composite material to fabricate 3D-printed scaffolds for bone tissue engineering. *Mater. Sci. Eng. C* **2021**, *118*, 111334. [[CrossRef](#)]
176. Liu, H.; Webster, T.J. Enhanced biological and mechanical properties of well-dispersed nanophase ceramics in polymer composites: From 2D to 3D printed structures. *Mater. Sci. Eng. C* **2011**, *31*, 77–89. [[CrossRef](#)]

177. Han, R.; Buchanan, F.; Ford, L.; Julius, M.; Walsh, P.J. A comparison of the degradation behaviour of 3D printed PDLGA scaffolds incorporating bioglass or biosilica. *Mater. Sci. Eng. C* **2021**, *120*, 111755. [[CrossRef](#)] [[PubMed](#)]
178. Yang, Y.; Yang, S.; Wang, Y.; Yu, Z.; Ao, H.; Zhang, H.; Qin, L.; Guillaume, O.; Eglin, D.; Richards, R.G.; et al. Anti-infective efficacy, cytocompatibility and biocompatibility of a 3D-printed osteoconductive composite scaffold functionalized with quaternized chitosan. *Acta Biomater.* **2016**, *46*, 112–128. [[CrossRef](#)] [[PubMed](#)]
179. Wiria, F.E.; Tay, B.Y.; Chandrasekaran, M.; Zhang, S.X.; Maleksaeedi, S.; He, Z. 3D Printing of customized biomedical scaffolds and implants. In Proceedings of the 1st International Conference on Progress in Additive Manufacturing, Singapore, 26–28 May 2014; pp. 411–416. [[CrossRef](#)]
180. Kim, E.V.; Petronyuk, Y.S.; Guseynov, N.A.; Tereshchuk, S.V.; Popov, A.A.; Volkov, A.V.; Gorshenev, V.N.; Olkhov, A.A.; Levin, V.M.; Dymnikov, A.B.; et al. Biocompatibility and Bioresorption of 3D-Printed Polylactide and Polyglycolide Tissue Membranes. *Bull. Exp. Biol. Med.* **2021**, *170*, 356–359. [[CrossRef](#)] [[PubMed](#)]
181. Ma, R.; Lai, Y.-X.; Li, L.; Tan, H.-L.; Wang, J.-L.; Li, Y.; Tang, T.-T.; Qin, L. Bacterial inhibition potential of 3D rapid-prototyped magnesium-based porous composite scaffolds—an in vitro efficacy study. *Sci. Rep.* **2015**, *5*, 13775. [[CrossRef](#)]
182. Ding, C.; Qiao, Z.; Jiang, W.; Li, H.; Wei, J.; Zhou, G.; Dai, K. Regeneration of a goat femoral head using a tissue-specific, biphasic scaffold fabricated with CAD/CAM technology. *Biomaterials* **2013**, *34*, 6706–6716. [[CrossRef](#)]
183. Kim, S.H.; Park, J.H.; Kwon, J.S.; Cho, J.G.; Park, K.G.; Park, C.H.; Yoo, J.J.; Atala, A.; Choi, H.S.; Kim, M.S.; et al. NIR fluorescence for monitoring in vivo scaffold degradation along with stem cell tracking in bone tissue engineering. *Biomaterials* **2020**, *258*, 120267. [[CrossRef](#)]
184. Panayotov, I.V.; Orti, V.; Cuisinier, F.; Yachouh, J. Polyetheretherketone (PEEK) for medical applications. *J. Mater. Sci. Mater. Med.* **2016**, *27*, 118. [[CrossRef](#)]
185. Sikder, P.; Ferreira, J.A.; Fakhrabadi, E.A.; Kantorski, K.Z.; Liberatore, M.W.; Bottino, M.C.; Bhaduri, S.B. Bioactive amorphous magnesium phosphate-polyetheretherketone composite filaments for 3D printing. *Dent. Mater.* **2020**, *36*, 865–883. [[CrossRef](#)]
186. Oladapo, B.I.; Zahedi, S.A.; Ismail, S.O. Mechanical performances of hip implant design and fabrication with PEEK composite. *Polymer (Guildf)* **2021**, *227*, 123865. [[CrossRef](#)]
187. Chen, X.; Wang, F.; Sun, F.; Zhang, L.; Wu, G. Digital fabrication of an adult speech aid prosthesis by using a 3-dimensionally printed polyetheretherketone framework. *J. Prosthet. Dent.* **2020**, *127*, 358–361. [[CrossRef](#)] [[PubMed](#)]
188. Deng, L.; Deng, Y.; Xie, K. AgNPs-decorated 3D printed PEEK implant for infection control and bone repair. *Colloids Surfaces B Biointerfaces* **2017**, *160*, 483–492. [[CrossRef](#)]
189. Oladapo, B.I.; Zahedi, S.A.; Ismail, S.O.; Omigbodun, F.T. 3D printing of PEEK and its composite to increase biointerfaces as a biomedical material- A review. *Colloids Surfaces B Biointerfaces* **2021**, *203*, 111726. [[CrossRef](#)] [[PubMed](#)]
190. Zheng, J.; Zhao, H.; Dong, E.; Kang, J.; Liu, C.; Sun, C.; Li, D.; Wang, L. Additively-manufactured PEEK/HA porous scaffolds with highly-controllable mechanical properties and excellent biocompatibility. *Mater. Sci. Eng. C* **2021**, *128*, 112333. [[CrossRef](#)] [[PubMed](#)]
191. Liu, D.; Fu, J.; Fan, H.; Li, D.; Dong, E.; Xiao, X.; Wang, L.; Guo, Z. Application of 3D-printed PEEK scapula prosthesis in the treatment of scapular benign fibrous histiocytoma: A case report. *J. Bone Oncol.* **2018**, *12*, 78–82. [[CrossRef](#)]
192. Basgul, C.; MacDonald, D.W.; Siskey, R.; Kurtz, S.M. Thermal localization improves the interlayer adhesion and structural integrity of 3D printed PEEK lumbar spinal cages. *Materialia* **2020**, *10*, 100650. [[CrossRef](#)] [[PubMed](#)]
193. Honigmann, P.; Sharma, N.; Schumacher, R.; Rueegg, J.; Haefeli, M.; Thieringer, F. In-Hospital 3D Printed Scaphoid Prosthesis Using Medical-Grade. *Biomed Res. Int.* **2021**, *2021*, 1301028. [[CrossRef](#)]
194. Honigmann, P.; Sharma, N.; Okolo, B.; Popp, U.; Msallem, B.; Thieringer, F.M. Patient-Specific Surgical Implants Made of 3D Printed PEEK: Material, Technology, and Scope of Surgical Application. *Biomed Res. Int.* **2018**, *2018*, 4520636. [[CrossRef](#)]
195. Feng, X.; Ma, L.; Liang, H.; Liu, X.; Lei, J.; Li, W.; Wang, K.; Song, Y.; Wang, B.; Li, G.; et al. Osteointegration of 3D-Printed Fully Porous Polyetheretherketone Scaffolds with Different Pore Sizes. *ACS Omega* **2020**, *5*, 26655–26666. [[CrossRef](#)]
196. Basgul, C.; Yu, T.; Macdonald, D.W.; Siskey, R.; Marcolongo, M.; Kurtz, S.M. Structure-property relationships for 3d-printed PEEK intervertebral lumbar cages produced using fused filament fabrication. *Mater. Res. Soc.* **2018**, *33*, 2040–2051. [[CrossRef](#)]
197. Guo, F.; Huang, S.; Hu, M.; Yang, C.; Li, D.; Liu, C. Biomechanical evaluation of a customized 3D-printed polyetheretherketone condylar prosthesis. *Exp. Ther. Med.* **2021**, *21*, 348. [[CrossRef](#)] [[PubMed](#)]
198. Feng, X.; Yu, H.; Liu, H.; Yu, X.; Feng, Z.; Bai, S.; Zhao, Y. Three-Dimensionally-Printed Polyether-Ether-Ketone Implant with a Cross-Linked Structure and Acid-Etched Microporous Surface Promotes Integration with Soft Tissue. *Int. J. Mol. Sci.* **2019**, *20*, 3811. [[CrossRef](#)] [[PubMed](#)]
199. Han, X.; Sharma, N.; Xu, Z.; Scheideler, L.; Geis-Gerstorfer, J.; Rupp, F.; Thieringer, F.M.; Spintzyk, S. An In Vitro Study of Osteoblast Response on Fused-Filament Fabrication 3D Printed PEEK for Dental and Cranio-Maxillofacial Implants. *J. Clin. Med.* **2019**, *8*, 771. [[CrossRef](#)] [[PubMed](#)]
200. Kang, J.; Wang, L.; Yang, C.; Wang, L.; Yi, C.; He, J.; Li, D. Custom design and biomechanical analysis of 3D-printed PEEK rib prostheses. *Biomech. Model. Mechanobiol.* **2018**, *17*, 1083–1092. [[CrossRef](#)] [[PubMed](#)]
201. Elhattab, K.; Sikder, P.; Walker, J.M.; Bottino, M.C.; Bhaduri, S.B. Fabrication and evaluation of 3-D printed PEEK scaffolds containing Macropores by design. *Mater. Lett.* **2020**, *263*, 127227. [[CrossRef](#)]

202. Su, Y.; He, J.; Jiang, N.; Zhang, H.; Wang, L.; Liu, X.; Li, D.; Yin, Z. Additively-manufactured poly-ether-ether-ketone (PEEK) lattice scaffolds with uniform microporous architectures for enhanced cellular response and soft tissue adhesion. *Mater. Des.* **2020**, *191*, 108671. [[CrossRef](#)]
203. Carpenter, R.D.; Klosterho, B.S.; Torstrick, F.B.; Foley, K.T.; Burkus, J.K.; Lee, C.S.D.; Gall, K.; Guldborg, R.E.; Safranski, D.L. Effect of porous orthopaedic implant material and structure on load sharing with simulated bone ingrowth: A finite element analysis comparing titanium and PEEK. *Behav. Biomed. Mater.* **2018**, *80*, 68–76. [[CrossRef](#)]
204. Basgul, C.; Yu, T.; Macdonald, D.W.; Siskey, R.; Marcolongo, M.; Kurtz, S.M. Does annealing improve the interlayer adhesion and structural integrity of FFF 3D printed PEEK lumbar spinal cages? *J. Mech. Behav. Biomed. Mater.* **2020**, *102*, 103455. [[CrossRef](#)] [[PubMed](#)]
205. Zhang, C.; Wang, L.; Kang, J.; Martel, O.; Li, D. Bionic design and verification of 3D printed PEEK costal cartilage prosthesis. *J. Mech. Behav. Biomed. Mater.* **2020**, *103*, 103561. [[CrossRef](#)]
206. Spece, H.; Yu, T.; Law, A.; Marcolongo, M.; Kurtz, S. 3D printed porous PEEK created via fused filament fabrication for osteoconductive orthopaedic surfaces. *J. Mech. Behav. Biomed. Mater.* **2020**, *109*, 103850. [[CrossRef](#)]
207. Kang, J.; Zhang, J.; Zheng, J.; Wang, L.; Li, D.; Liu, S. 3D PEEK implant for mandibular defects repair—A new method. *J. Mech. Behav. Biomed. Mater.* **2021**, *116*, 104335. [[CrossRef](#)] [[PubMed](#)]
208. Li, S.; Wang, T.; Hu, J.; Li, Z.; Wang, B.; Wang, L. Surface porous poly-ether-ether-ketone based on three-dimensional printing for load-bearing orthopedic implant. *J. Mech. Behav. Biomed. Mater.* **2021**, *120*, 104561. [[CrossRef](#)] [[PubMed](#)]
209. Oladapo, B.I.; Zahedi, S.A.; Chong, S.; Omigbodun, F.T.; Malachi, I.O. 3D printing of surface characterisation and finite element analysis improvement of tensile properties for PEEK-HAP-GO in bone implant. *Int. J. Adv. Manuf. Technol.* **2019**, 1–3.
210. Zhu, C.; He, M.; Sun, D.; Huang, Y.; Huang, L. 3D printed multifunctional PEEK bone scaffold for multimodal treatment of osteosarcoma and osteomyelitis. *ACS Appl. Mater. Interfaces* **2021**, *40*, 47327–47340. [[CrossRef](#)] [[PubMed](#)]
211. Deng, Y.; Shi, X.; Chen, Y.; Yang, W.; Ma, Y.; Shi, X.-L.; Song, P.; Dargusch, M.S.; Chen, Z.-G. Bacteria-Triggered pH-Responsive Osteopotentiating Coating on 3D-Printed Polyetheretherketone Scaffolds for Infective Bone Defect Repair. *Ind. Eng. Chem. Res.* **2020**, *59*, 12123–12135. [[CrossRef](#)]
212. Alam, F.; Varadarajan, K.M.; Koo, J.H.; Wardle, B.L.; Kumar, S. Additively Manufactured Polyetheretherketone (PEEK) with Carbon Nanostructure Reinforcement for Biomedical Structural Applications. *Adv. Eng. Mater.* **2020**, *22*, 2000483. [[CrossRef](#)]
213. Jung, H.; Jang, T.; Lee, J.E.; Park, S.J.; Son, Y.; Park, S. Enhanced bioactivity of titanium-coated polyetheretherketone implants created by a high-temperature 3D printing process. *Biofabrication* **2019**, *11*, 045014. [[CrossRef](#)]
214. Oladapo, B.I.; Ismail, S.O.; Bowoto, O.K.; Omigbodun, F.T.; Olawumi, M.A.; Muhammad, M.A. Lattice design and 3D-printing of PEEK with Ca₁₀(OH)(PO₄)₃ and in-vitro bio-composite for bone implant. *Int. J. Biol. Macromol.* **2020**, *165*, 50–62. [[CrossRef](#)]
215. Oladapo, B.I.; Zahedi, S.A. Improving bioactivity and strength of PEEK composite polymer for bone application. *Mater. Chem. Phys.* **2021**, *266*, 124485. [[CrossRef](#)]
216. Manzoor, F.; Golbang, A.; Jindal, S.; Dixon, D.; Mcilhagger, A.; Harkin-jones, E.; Crawford, D.; Mancuso, E. 3D printed PEEK/HA composites for bone tissue engineering applications: Effect of material formulation on mechanical performance and bioactive potential. *J. Mech. Behav. Biomed. Mater.* **2021**, *121*, 104601. [[CrossRef](#)]